Check for updates

Non-thermal plasma catalysis for conversion of CO_2 and CH_4 to oxygenates: a mini review

Liangpang Xu, [iD]†[a] Yi Xie,†[a] Bichao Wu,[a] Qian Lu,[a] Lu Wang [iD][b] and Ying Wang [iD]*[a]

Non-thermal plasma (NTP) is an emerging technology for the conversion of CO_2 and CH_4 under mild conditions. This mini review systematically summarizes recent advances in NTP catalysis for the direct conversion of CO_2 and CH_4 into value-added oxygenates, with a focus on two key aspects: catalyst design and reactor optimization. The metal active sites (e.g., Cu, Ni, Co) and their properties (valence state, dispersion) are critical in directing reaction pathways towards specific oxygenates like alcohols or acids, while the support material modulates performance by influencing the local electric field and stabilizing intermediates. Dielectric barrier discharge (DBD) reactors are predominant, and innovations in reactor structure, electrode design (e.g., water electrodes, surface microdischarge), and configuration (e.g., plasma bubble reactors) are crucial for enhancing efficiency and selectivity, even enabling long-chain hydrocarbon formation. Despite progress, challenges in selectivity and energy efficiency remain. Future efforts should focus on rational catalyst design and advanced reactor integration to advance the industrial application of NTP for greenhouse gas valorization.

1 Introduction

Mitigating climate change relies on technologies that can reduce greenhouse gas emissions and convert them into valuable products.[1,2] Among the greenhouse gases, methane (CH_4) and carbon dioxide (CO_2) are particularly consequential: CH_4 has a high global warming potential over a short time period,[3] while CO_2 is the dominant long-lived forcing agent in the atmosphere.[4] Simultaneously converting these two abundant yet thermodynamically stable gases into value-added oxygenates such as alcohols and acids is a compelling pathway to close the carbon loop while creating economic value.[5,6]

Traditional thermal catalysis is typically indirect and relies on a two-step sequence: (1) dry reforming of methane (DRM) at high temperatures (>700 °C) to generate syngas (CO and H_2),[7,8] and (2) high-pressure conversion of syngas to fuels and chemicals.[9] Despite technological maturity, this route is

[a] Department of Chemistry, The Chinese University of Hong Kong, Hong Kong S. A. R., China. E-mail: ying.b.wang@cuhk.edu.hk

[b] School of Science and Engineering, The Chinese University of Hong Kong (Shenzhen), Shenzhen, China

† These authors contributed equally to this work.

Dr. Liangpang Xu received his Ph.D. in 2022 from The Chinese University of Hong Kong (CUHK) under the supervision of Prof. Jimmy C. Yu. He is currently a research assistant in the Department of Chemistry at CUHK. His research focuses on photocatalysis for artificial photosynthesis and environmental remediation, as well as plasma technology for the conversion of greenhouse gases into high-value chemicals.

Liangpang Xu

Yi Xie received her Ph.D. in Chemistry from The Chinese University of Hong Kong (CUHK) in 2023, earning the Young Scholars Thesis Award. She is currently conducting postdoctoral research in the Department of Chemistry at CUHK. Her research focuses on electrocatalysis and CH_4/CO_2 conversion, with a dedication to translating fundamental research into scalable, practical systems.

Yi Xie

energy intensive, depends on fossil heat and H_2, and causes significant CO_2 emissions. Biological approaches rely on the precise action of enzymes, but suffer from low volumetric productivity, large land footprint, and high water and nutrient consumption.[10] Recently, chemical methods powered by renewable energy have attracted increasing attention for carbon-neutral conversion. Photo- and electro-catalytic approaches have been widely reported for CH_4 oxidation or CO_2 reduction to various oxygenates.[11,12] Despite their potential, the conversion efficiency is still highly restrained due to the fundamental challenges in breaking strong C–H bonds in CH_4 and activating linear CO_2 molecules.[11,13,14]

Non-thermal plasma (NTP) has emerged as a promising approach for direct co-conversion of CO_2 and CH_4 into oxygenates under mild conditions.[15–19] The highly energetic electrons (typically at 1–10 eV) can simultaneously activate CO_2 and CH_4 via excitation, ionization, and dissociation at near-ambient gas temperatures.[20] The resulting intermediates such as radicals and ions then freely recombine to form various products including oxygenates. Although NTP shows considerable promise, significant challenges remain for efficient conversion of CO_2 and CH_4 into oxygenates. Uncontrolled recombination of reactive species restricts overall oxygenate selectivity (typically <15%) and impedes the targeted formation of specific products.[21,22] In addition, energy efficiency is low because a substantial portion of input energy is consumed in generating high-energy electrons and sustaining background plasma processes rather than being effectively utilized for reactant activation. Integrating catalysts with NTP offers a viable strategy to address these issues by lowering apparent activation barriers, tuning surface energetics, and directing reaction pathways toward desired products.[23,24] Reactor design further plays a critical role in affecting discharge characteristics and reaction mechanisms.[25] Considerable efforts have been devoted to

rational catalyst and reactor engineering to advance CO_2/CH_4 co-conversion.[25,26] A comprehensive review of these developments is therefore essential to consolidate current achievements, identify remaining gaps, and guide future research toward industrial implementation.

While previous reviews have extensively covered the fundamentals and broad applications of plasma catalysis,[27–29] a dedicated analysis targeting the direct and selective one-step synthesis of liquid oxygenates from CO_2 and CH_4 – encompassing integrated advances in catalyst design, reactor engineering, and interface mechanisms – remains insufficiently addressed. Here, we provide a systematic review of NTP technology for the conversion of CO_2 and CH_4 into oxygenates, focusing on both catalyst design and reactor optimization. The mechanisms of NTP-catalyzed reactions are first elucidated. We further analyze the two key components of catalysts – metal active sites and the support environment, to highlight the structure–activity relationships under plasma conditions to outline fundamental principles for catalyst design. In addition, a detailed analysis of reactor design is presented, covering structural configuration, electrode material selection, and reactor setup. Finally, we outline future perspectives for the co-conversion of CO_2 and CH_4 into oxygenates via NTP technology, addressing key challenges in selectivity and energy efficiency, with the goal of advancing the application of NTP in greenhouse gas conversion in the future.

2 Fundamentals of plasma catalytic CO_2/CH_4 conversion

2.1 Plasma and its characteristics

Plasma, often described as the fourth state of matter, is a partially or fully ionized gas consisting of electrons, ions, radicals, and excited molecules.[30] It exhibits collective electromagnetic behaviour and is commonly categorized as either thermal plasma or NTP, depending on the relationship between the electron temperature (T_e) and the heavy-particle temperature (T_h). In thermal plasmas, T_e is similar to T_h and the system approaches thermodynamic equilibrium, typically reaching several thousand kelvins. In contrast, NTP operates far from equilibrium, with T_e (1–10 eV, 10^4–10^5 K) far exceeding T_h (near room temperature).[31] These energetic electrons can efficiently break strong covalent bonds without significantly heating the bulk gas. This unique nature enables chemical transformations under mild macroscopic conditions while maintaining highly energetic micro-environments.[32] It makes NTP particularly effective for the low-temperature activation of thermodynamically stable molecules of CO_2 and CH_4 with the large bond energy of C=O (E_{diss} = 5.5 eV) and C–H (E_{diss} = 4.5 eV). Besides, electron density (N_e) and T_e are essential for describing NTP activation. Specifically, under representative atmospheric-pressure dielectric barrier discharge (DBD) operating conditions, the electron density typically ranges from 10^{18}–10^{21} m^{-3}.[33]
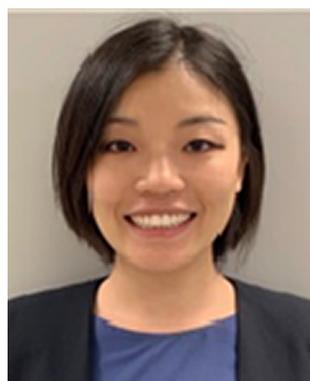
Ying Wang received her Ph.D. in Electrochemistry from the University of Oxford under the supervision of Prof. Richard G. Compton. Before joining The Chinese University of Hong Kong (CUHK), she worked as a postdoctoral research fellow in electrocatalysis in the United States and Canada. She is currently an Associate Professor in the Department of Chemistry at CUHK. Her research group focuses on carbon conversion through electrocatalysis and plasma catalysis, aiming to develop sustainable pathways for carbon utilization and energy transformation.
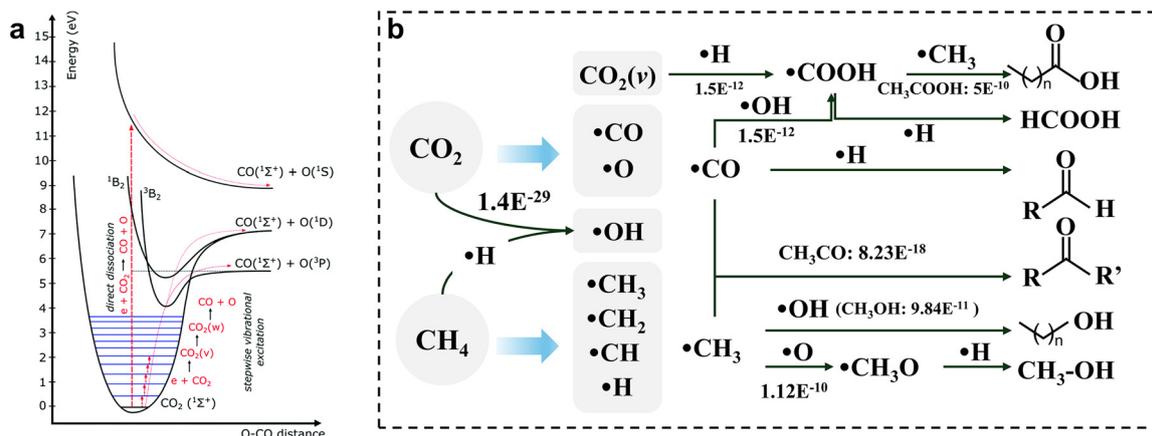
Ying Wang

Fig. 1 (a) Energy-level diagram for CO_2 electronic and vibrational modes.[24] Copyright 2017, Royal Society of Chemistry; (b) overview diagram illustrating the potential reaction routes for the formation of oxygenate products in CH_4 and CO_2 plasma. The numbers in (b) represent the reported rate coefficient, m³ per molecule per s.[15]

2.2 Reaction mechanism for NTP-driven CO_2/CH_4 conversion

NTP, especially atmospheric-pressure DBD, is the most widely used configuration for the conversion of CO_2 and CH_4 into oxygenates. The plasma environment introduces a complex network of electron-induced and radical-mediated reactions that fundamentally differ from those in thermal catalysis. In the discharge zone, energetic electrons accelerated under oscillating electric fields collide with neutral gas molecules, transferring energy through inelastic collisions. These collisions induce excitation, ionization, dissociation, and vibrational activation, thereby producing a complex mixture of transient species.[34] The distinct activation efficiencies of CO_2 and CH_4 in plasma environments arise from differences in both molecular structure and excitation pathways.[20]

As shown in Fig. 1a, CO_2 dissociation can proceed *via* direct electronic excitation at high electron energies (>7 eV) or stepwise vibrational excitation.[24] In the latter route, CO_2 climbs the "vibrational ladder" through successive low-energy excitations, eventually reaching the dissociation limit at an overall activation energy of approximately 5.5 eV. Because the input energy closely matches the C=O bond energy and is channeled into vibrational modes rather than electronic excitation, this pathway can be highly energy-efficient and is considered a key channel in warm and certain non-thermal discharges. The practical significance of vibrational excitation depends on plasma parameters. The vibrational excitation pathway is especially efficient in plasmas like gliding arc, microwave, and certain radio-frequency discharges, where energy can be selectively channeled into vibrational modes.[24] In DBD, both direct electronic excitation and vibrational mechanisms can contribute, with their relative importance influenced by specific operating conditions (*e.g.*, specific energy input, gas composition).[24] CO_2 fragmentation predominantly produces ·CO and ·O radicals or vibrationally excited CO_2 molecules. These reactive species trigger a cascade of radical chain reactions and secondary recombination step.

By contrast, under typical atmospheric-pressure DBD plasma for CH_4 and CO_2 conversion, the vibrational activation of CH_4 is inefficient due to its complex vibrational spectrum and unfavourable energy coupling with the electron energy distribution.[35] The stretching and bending modes of the C–H bonds do not couple effectively with typical plasma electron energies, and CH_4 vibrationally excited states exhibit very short lifetimes, undergoing rapid vibrational-to-translational relaxation.[36] As a consequence, vibrational energy is quickly converted into heat rather than being accumulated stepwise, and CH_4 cannot effectively undergo ladder-climbing dissociation. Electron-impact dissociation of CH_4 therefore proceeds mainly *via* direct electronic excitation, yielding abundant ·CH_3 radicals together with smaller amounts of ·CH_2 and ·CH species. These reactive species trigger a cascade of radical chain reactions and secondary recombination steps, underpinning the complex chemistry of NTP-driven CO_2/CH_4 conversion. It should be noted, however, that CH_4 can also undergo substantial vibrational excitation in appropriately designed plasma environments, particularly under low-pressure or microwave discharge conditions – where pronounced vibrational nonequilibrium behavior has been experimentally observed.[35] Furthermore, vibrationally excited species such as CO_2(v), as well as plasma-activated catalyst surfaces, can transfer energy to CH_4 through Eley–Rideal interactions or enhanced vibrational–vibrational coupling, thereby opening alternative activation pathways in plasma-catalytic systems.[37]

Various oxygenated products can be produced in NTP-driven CO_2/CH_4 systems, including methanol (CH_3OH), formic acid (HCOOH), ethanol (CH_3CH_2OH), acetic acid (CH_3COOH), *etc.* (Fig. 1b, Table 1).[23,24] Methanol is the dominant C_1 oxygenate in most plasma-catalytic systems, formed through reactions between ·CH_3 radicals and O-containing intermediates (*e.g.* ·O, ·OH species). Alternatively, methanol may arise *via* a CO_2 reduction pathway involving successive hydrogenation of CO_2 through formate-type intermediates (CO_2 + ·H → HCOO· → CH_3O· → CH_3OH). Ethanol formation

Table 1 Non-thermal plasma catalytic performance of representative catalysts for the direct conversion of CH_4 and CO_2 to oxygenates

| Catalyst | Experimental conditions | | | | Conversion (%) | | Energy efficiency | Main liquid products and selectivity (%) | Liquid selectivity (%) | Ref. |
	CO_2/CH_4	Plasma	Reactor	Power (W)	CO_2	CH_4				
Cu/γ-Al_2O_3	1	DBD	3 mm gap, 45 mm length	10	15.4	18.3	—	CH_3COOH (40.2), CH_3OH, C_2H_5OH, C_3H_6O	59.1	15
Fe–SiO_2	2 : 1	DBD	3 mm gap, 45 mm length	~10	~34.5	~45.5	~20.5 (SIE)	CH_3OH (31), CH_3COOH (12.4), C_2H_5OH	~40.0	16
Co–SiO_2					~33.5	~47.5	~21 (SIE)	CH_3OH (20.5), CH_3COOH (17.9), C_2H_5OH		
—	1 : 1	DBD	Temperature-controlled water electrode	15	29.0	~32.0	0.83 mol kWh^{-1} (CH_3OH)	CH_3OH (43)	60.0	40
$Cu/Al(OH)_3$	1 : 1	DBD	3 mm gap, 45 mm length	5	~17	~7	—	CH_3OH (22), C_2H_5OH (14), C_3H_8O	~44%	41
K-Fe/C-SiO_2	1 : 1	DBD	3.5 mm gap, 150 mm length	2.37	5.17	15.34	0.58 mmol kJ^{-1}	CH_3COOH (12.97), C_{3+} acid (7.35), CH_3OH, C_2H_5OH	21.76	42
NiGa/NF	1 : 1	DBD	2.25 mm gap, 50 mm length	25	8.5	16.0	0.168 mmol kJ^{-1}	CH_3COOH (17.8), CH_3OH (~6.2), C_2H_5COOH	~34	43
Ni/HZSM-5	1 : 1	DBD	3 mm gap, 45 mm length, water electrode	18	~2.3	~4	—	Alcohols (C_1–C_4), CH_3COOH, C_3H_6O, aldehyde	45	44
Ni–Fe/Al_2O_3	—	DBD	2 mm gap	23	19.7	34.8	—	CH_3COOH (23.9), CH_3OH (19.1), CH_3CH_2OH (14.5), C_3H_8O (15.7), C_2H_5COOH (16.3), HCHO (10.5) (in liquid)	38.6	45
CuSA-CN	1 : 1	DBD	—	10	7.31	11.58	0.28 mmol kJ^{-1}	CH_3COOH (11.85), CH_3OH (5.08), C_2H_5OH, C_3H_7OH, C_2H_5COOH	—	46
Cu/5A	1 : 1 (with trace water)	DBD	2 mm gap, 60 mm length	36	~23	~40	73.6 kJ L^{-1}	CH_3OH (~18%), C_2H_5OH (5.08), CH_3COOH, C_3H_8O	26	47
Cu/UiO-66-NH_2	1 : 1	DBD	—	20	21.6	23.5	—	CH_3OH (20.9), C_2H_5OH (18.4) C_3H_6O(8.6), CH_3COOH (3.3), CH_3CHO (2.3)	53.4	48
Fe_2O_3/g-C_3N_4	1 : 1	DBD	3 mm gap, 50 mm length	20	18	22	0.35 mmol kJ^{-1}	CH_3OH (24.4%), C_2H_5OH (5.08)	40.1	49
Au-HZSM-5	1 : 1	DBD	3 mm gap, 40 mm length	12	~12	~20	—	R-COOH, R-OH, R-CO-R, R-CHO	~32	50
P-CoMgAl/NF	1 : 1	DBD	50 mm length	—	~10.5	~16	0.16 mmol kJ^{-1}	C_2H_5OH, CH_3OH, $C_3H_6O_2$, C_2H_5OH	40	31

requires C–C coupling between C_1 fragments, typically through reactions between $\cdot CH_3$ and $\cdot CH_2OH$ species. Acetic acid is generally produced *via* the coupling of $\cdot CH_3$ with $\cdot COOH$ or bicarbonate (HCO_3^-) intermediates.

In plasma-only systems, the short lifetimes of radicals (micro- to milliseconds) and the absence of defined surface sites lead to largely random gas-phase interactions, multiple parallel pathways and extensive oxidation or cracking.[24] As a result, plasma alone usually yields broad product distributions and modest energy efficiency. Coupling NTP with heterogeneous catalysis (plasma catalysis) can effectively overcome these limitations. In such hybrid systems, the plasma rapidly activates CO_2 and CH_4, whereas

the catalyst offers active sites that stabilize key intermediates and steer the reaction toward desired products. On the catalyst surface, plasma-generated radicals, ions and excited species predominantly react *via* Eley–Rideal (E–R) and Langmuir–Hinshelwood (L–H) mechanisms.[38,39] In the E–R mechanism, a gas-phase radical directly collides with and reacts with an adsorbed species, forming products through a low-barrier pathway. In the L–H mechanism, two adsorbed intermediates diffuse on the surface and react with each other. The interplay between these plasma-driven gas-phase reactions and surface catalytic steps is crucial for achieving selective and energy-efficient CO_2/CH_4 conversion to oxygenates.

2.3 Synergy between plasma and catalysts

The combination of NTP with heterogeneous catalysis effectively overcomes key limitations of plasma-only systems, notably poor selectivity and energy efficiency. In these hybrid systems, catalysts are positioned within or directly adjacent to the plasma discharge. The plasma rapidly activates stable CO_2 and CH_4, generating a continuous flux of reactive radicals (*e.g.*, $\cdot CH_3$, $\cdot OH$), excited molecules, and ions. These short-lived species are efficiently delivered to the catalyst surface *via* electric-field-driven transport and enhanced mixing. The catalyst then provides active sites to capture and stabilize these intermediates (*e.g.*, $\cdot CH_{3ads}$ and $\cdot COOH_{ads}$), thereby guiding surface reactions toward the desired oxygenated products.

2.3.1 Surface processes for guiding and stabilizing reactive species. Plasma generates abundant short-lived radicals (*e.g.*, $\cdot CH_3$, $\cdot OH$, $\cdot COOH$), excited molecules, ions, and vibrationally activated species whose gas-phase lifetimes typically fall within microseconds to milliseconds. These species undergo rapid collisions that often lead to non-selective recombination and energy loss. Catalysts provide structured surfaces capable of intercepting and stabilizing these transient intermediates through chemisorption, electrostatic interactions, and defect trapping.[51] Although short-lived, the plasma species are continuously produced and achieve efficient transport to the catalyst surface *via* electric-field-driven migration, microscale convection induced by ionic wind, and enhanced gas-phase mixing.[52,53] Metal sites such as Cu^+ and Co^0 can strongly bind $\cdot CH_3$, whereas oxygen vacancies or Lewis acid sites effectively anchor $\cdot COOH$ or activated CO_2. Converting gas-phase radicals into adsorbed intermediates significantly extends their chemical lifetime and increases the probability of controlled bond-forming processes. Two key mechanisms enable catalyst surfaces to guide reactions selectively: the E–R mechanism and L–H mechanism, as abovementioned.

Beyond classical radical stabilization, plasma-catalytic systems benefit from additional electronically driven surface processes. Plasma emission or external illumination can generate localized electrons on semiconductor catalysts such as TiO_2 and ZnO, which then interact with plasma-generated radicals and lower activation barriers.[54,55] Functionalized nanocarbons (*e.g.*, doped graphene, CNTs) can accumulate transient surface charge under plasma exposure, creating strong local electric fields that polarize adsorbates and modify reaction trajectories.[56] Additionally, plasmonic catalysts such as ordered Au or Ag nanoparticles on TiO_2 offer unique near-field enhancement, hot-electron injection, and photothermal activation pathways. Experiments in plasma-illuminated Au/TiO_2 systems demonstrate light-plasma synergy that enhances CH_4 activation and alters microdischarge behavior.[57] Meanwhile, plasmon-enabled resonance energy transfer mechanisms (*e.g.*, PC-RET) provide a valid conceptual basis for coupling plasmonic fields with reactive plasma species.[58,59]

2.3.2 Effects of the plasma on the catalyst. Plasma exerts multifaceted effects on catalysts, driving synergistic enhancements in catalytic performance.[60] It induces morphological changes, increasing catalyst dispersion and specific surface area by mitigating sintering *via* energetic particle bombardment. Chemically, plasma dynamically alters catalyst oxidation states and modifies electronic properties like work function. On the surface, it reduces coke formation and catalyst poisoning by facilitating the removal of blocking species.

For example, Guo *et al.* reported that exposure of manganese oxide catalysts to DBD plasma reduced granularity and increased dispersion, thereby enlarging the specific surface area and creating more active sites (*e.g.*, vacancies, edges, and corner atoms), which enhances catalytic reactivity.[61] Similarly, plasma can modify the oxidation state of catalysts. In plasma-assisted DRM, studies by Gallon *et al.*[62] and Tu *et al.*[63] observed the reduction of NiO to metallic Ni under plasma treatment. The plasma-enabled formation of highly dispersed, ultrasmall Ni nanoparticles significantly improves catalytic activity at low temperatures, enhances CO_2 adsorption, mitigates coking through size effects, and ensures exceptional long-term stability.[64]

In plasma-assisted co-conversion of CH_4 and CO_2, the highly reactive environment can significantly alter Ni- or Cu-based catalysts, inducing surface oxidation, reduction, sintering, or phase transformations. For instance, Ni^0 can be partially oxidized to NiO, while Cu may cycle between Cu^0 and Cu^+/Cu^{2+} states. Such changes can either deactivate the catalyst by blocking active sites or, conversely, enhance activity by promoting redox dynamics and improving carbon resistance. The net effect on catalytic performance depends on plasma parameters, catalyst structure, and gas composition. Therefore, the dynamic structural evolution of metal nanoparticles in CO_2/CH_4 plasma catalysis is an important aspect worthy of deeper investigation.

2.3.3 Energy resonance and coupling with vibrationally excited states. Directly applying thermal catalyst design principles is constrained by the fundamental differences in activation mechanisms (energetic electrons/vibrationally excited species *vs.* thermal phonons). In recent years, while some studies utilize plasmonic responses for *in situ* monitoring of catalyst surface states during plasma processing,[65] the "non-thermal" synergistic mechanisms in plasma-catalyst systems have attracted significant attention, with vibrationally excited molecules (*e.g.*, $CO_2(v)$, $N_2(v)$) regarded as key mediators linking plasma physics and surface chemistry.[66] Low-temperature plasmas can selectively inject energy into molecular vibrational states, generating high-energy nonequilibrium species that markedly lower activation barriers for surface reactions (*e.g.*, dissociation, hydrogenation), enabling efficient conversion near room temperature.[67,68]

More intriguingly, when these vibrationally excited molecules interact with nanocatalysts exhibiting localized surface plasmon resonance (LSPR) (*e.g.*, Au, Ag), additional synergy may arise: plasmon decay produces hot electrons or

strong localized fields that promote adsorbate polarization and, *via* electron-vibration coupling, excite vibrational modes.[69] If gas-phase vibrational energy matches surface excited states, resonant energy transfer may occur, enhancing efficiency and selectivity.[70,71] Although this "vibration-plasmon" synergy remains entangled with thermal and radical effects, it represents a core non-thermal pathway, offering new strategies for designing low-energy plasma-assisted catalytic systems.

2.4 Energy efficiency

In plasma catalysis, energy efficiency (EE) is a key metric for evaluating the economic viability and feasibility of the process. It assesses how much of the input electrical energy is effectively utilized to generate the desired products. Because plasma involves multiple energy-consuming pathways such as gas ionization and excitation, its EE is typically far lower than that of conventional thermal catalysis, making accurate evaluation critically important.

There are several primary methods and related metrics used to assess energy efficiency:

$$EE\,(\%) = \frac{\chi_{Total} \times \Delta H^{o}_{298K}\,(kJ\,mol^{-1})}{SEI\,(kJ\,mol^{-1})} \quad (1)$$

$$= \frac{\chi_{Total} \times \Delta H^{o}_{298K}\,(eV\,per\,molecule)}{SEI\,(eV\,per\,molecule)}$$

$$SEI\,(kJ\,L^{-1}) = \frac{Power\,(kW) \times 60\,(s\,min^{-1})}{Flow\,rate\,(L\,min^{-1})} \quad (2)$$

The standard reaction enthalpy for pure CO_2 dissociation is 283 kJ mol^{-1} (equivalent to 2.93 eV per molecule), whereas for the DRM reaction, it is 247 kJ mol^{-1} (or 2.56 eV per molecule). The SEI and P are the specific energy input and plasma power (W), respectively.

Energy consumption (EC) refers to the amount of energy required to carry out the reaction and is typically expressed in terms of energy per mole or per molecule converted (in units of kJ mol^{-1} or eV per molecule):

$$EC\,(kJ\,mol^{-1}_{conv}) = \frac{SEI\,(kJ\,L^{-1}) \times 24.5\,(L\,mol^{-1})}{\chi_{Total}} \quad (3)$$

Note that the value of 24.5 L mol^{-1} applies only to ideal gases at 298 K and 1 atm.

To convert energy consumption into eV, the following relationship is used:

$$EC\,(kJ\,per\,molecule_{conv}) = EC\,(kJ\,mol^{-1}_{conv})$$

$$\times \frac{6.24 \times 10^{21}\,(eV\,kJ^{-1})}{6.022 \times 10^{23}\,(molecule\,per\,mol)} \quad (4)$$

Compared with conventional thermal catalysis, NTP-catalysis still faces key challenges, particularly limited energy efficiency and product selectivity (Table S1), and thus is not a direct replacement but rather a complementary technology suited for specific scenarios. Its unique niche stems from the ability to activate inert molecules (such as CO_2, N_2, and CH_4) under mild, near-ambient conditions, enabling reaction pathways inaccessible to thermal approaches. This advantage positions NTP for promising applications, including coupling with intermittent renewable energy sources to enhance economic viability, enabling modular and distributed small-scale chemical production (*e.g.*, gas upgrading), and potentially revolutionizing the synthesis of high-value chemicals where process flexibility and tunability outweigh raw conversion efficiency. Realizing this potential requires focused efforts to deepen understanding of plasma–catalyst interactions, selectively channel energy into desired reaction channels, and overcome scale-up barriers such as discharge uniformity and thermal management through advanced diagnostics and modelling. Bridging these gaps is essential to transition NTP-catalysis from laboratory research toward industrial implementation.

3 Catalyst design for oxygenate synthesis

In conventional thermal catalysis, oxygenate synthesis proceeds *via* surface-adsorbed intermediates governed by thermodynamic equilibrium and L–H mechanisms, relying on a uniform catalytic surface to activate stable reactants. In stark contrast, NTP generates a rich cocktail of reactive species including vibrationally excited molecules (*e.g.*, $CO_2(v)$), radicals, ions, and metastables at near-ambient temperatures. Consequently, the primary function of a plasma-catalyst shifts from "activating stable reactants" to "selectively capturing, stabilizing, and steering transient plasma-generated species toward desired products". This paradigm demands a fundamental rethinking of traditional catalyst design: composition, oxidation state, defect structure, and support properties must now be optimized not only for surface chemistry but also for synergistic coupling with plasma physics. Critically, the plasma-generated localized electric fields fundamentally alter the adsorption and distribution of active species, contrasting sharply with the electrically uniform surfaces in thermal catalysis. Thus, effective plasma catalyst design must integrate surface science with plasma physics, emphasizing charge modulation, field-enhanced activation, and the stabilization of short-lived intermediates to achieve superior activity and selectivity under non-equilibrium conditions.

Within this plasma-specific framework, the structural design of catalysts becomes critical for enhancing the adsorption and reaction of plasma-derived active species involved in CH_4 and CO_2 activation-processes that ultimately govern oxygenate selectivity.[72] Currently, catalysts employed in NTP technology are predominantly supported catalysts, which primarily consist of two key components: the metal active sites and the support (Table 1). The selection of metals

(such as Cu, Ni, Co, Fe metals) primarily determines the reaction pathway, while their structural properties including valence state, particle size, and dispersion also significantly influence the reaction selectivity and activity. The support, beyond the basic role of metal loading, can also alter the plasma discharge characteristics, modulate the electronic structure of active species, and provide essential acid–base sites. This synergistic interaction between the metal active sites and support collectively creates the "active center" for oxygenate generation within the plasma environment. In this section, we systematically introduce widely studied metals for CO_2/CH_4 conversion, including Cu-, Ni-, and Co-based

systems, as well as other representative metals. Furthermore, we discussed the influences of support in modulating the metal active sites and its impact on the plasma-catalytic performance.

3.1 Metal catalyst

The composition and electronic structure of the metal active sites are critical in determining reaction pathways. It is essential to avoid metal centers that exhibit excessively strong adsorption – leading to syngas formation and coke deposition, or excessively weak adsorption, which cannot
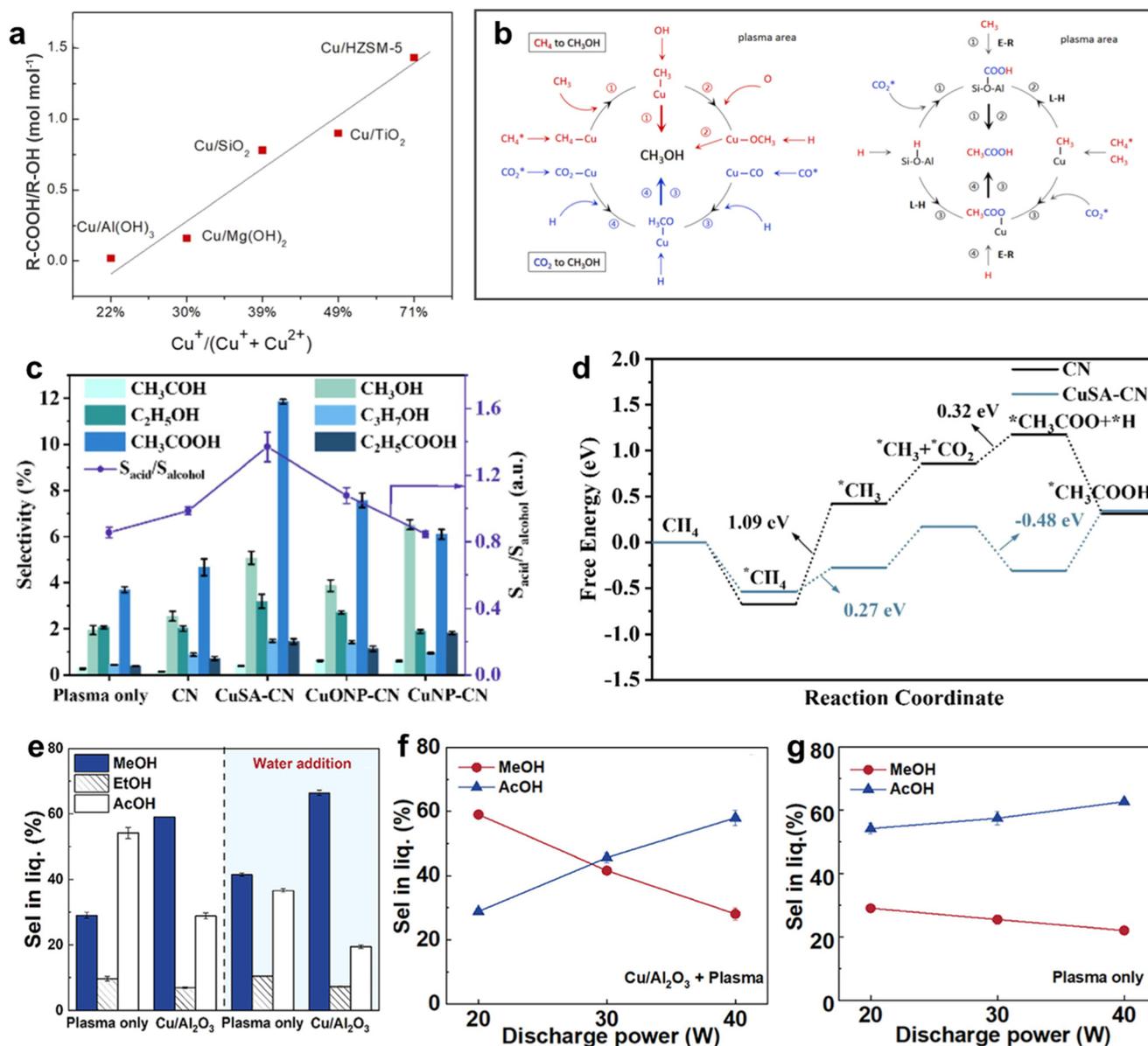

Fig. 2 (a) The mole ratio of R-COOH/R-OH (CH_3COOH/C_1–C_4OH) as a function of Cu^+ percentage; (b) possible reaction pathways for plasma-catalytic conversion of CO_2 and CH_4 to CH_3OH and CH_3COOH.[73] Copyright 2022, Elsevier; (c) selectivity of oxygenates and relative selectivity of acid to alcohol for Cu-SA-CN; (d) calculated free-energy diagram for CH_4 and CO_2 to generate CH_3COOH on CN and Cu-SA.[46] Copyright 2024, Elsevier; (e) effect of water addition on the selectivity for methanol and acetic acid and effect of discharge power on the selectivity for methanol and acetic acid in the (f) Cu/Al_2O_3 + plasma case and (g) plasma-only case.[75] Copyright 2025, American Chemical Society.

effectively stabilize intermediates derived from CO_2 and CH_4 dissociation. In NTP catalysis, Cu-based, Ni-based, Co-based, and some other metal-based catalysts have been widely studied.

3.1.1 Cu-based catalysts. Cu-based catalysts play a pivotal role in tuning the product distribution during the plasma-catalytic conversion of CH_4 and CO_2 into value-added oxygenates such as alcohols and acetic acid. The Cu valence state (Cu^{2+} vs. Cu^+) is critical in directing the reaction pathway. Unlike thermal CO_2 hydrogenation to methanol, where Cu^0 and Cu^+ dominate, plasma-catalytic studies consistently identify Cu^{2+} as the most selective state for CH_3OH, while Cu^+ promotes acetic acid formation (Fig. 2a and b).[73,74] This counterintuitive trend stems from the abundant ·CH_3 and ·OH radicals generated in NTP. Cu^{2+}, with its strong Lewis acidity, readily adsorbs ·OH or reacts with plasma-generated H_2O to form surface OH groups. These sites then rapidly combine with gas-phase ·CH_3 via an E–R mechanism to produce CH_3OH – a pathway kinetically inaccessible in thermal systems. In contrast, Cu^+ stabilizes ·COOH intermediates, promoting C–C coupling toward ethanol or acetate. Thus, the optimal Cu oxidation state in plasma catalysis is determined not by CO_2 adsorption strength (as in thermal catalysis) but by radical affinity and E–R reactivity.

For instance, in $Cu/Al(OH)_3$ catalysts calcined at 540 °C with 5 wt% Cu loading, the strong redox capacity and abundant Cu^{2+} species led to high alcohol selectivity of >38%.[41] In contrast, Cu/HZSM-5 with a high proportion of

Cu^+ species significantly enhanced acetic acid selectivity, aided by the presence of Brønsted acid sites (BAS) in HZSM-5 supports which facilitate CO_2 protonation and C–C coupling.[73]

The coordination structure of Cu active sites also influences catalytic performance. Single-atom Cu catalysts (CuSA) with a $Cu–N_4$ coordination structure anchored on carbon nitride (CuSA-CN) not only accelerate the activation of CH_4 and CO_2 but also lower the energy barriers for CH_4 dissociation and C–C coupling, thereby promoting acetic acid formation (Fig. 2c).[46] DFT calculations revealed that the energy barrier for the key step of *CH_3 and *CO_2 coupling to form *CH_3COO is significantly reduced on CuSA-CN compared to the bare support without Cu active sites (Fig. 2d), leading to a higher selectivity toward acetic acid.

Moreover, external conditions such as water addition and discharge power can further tailor the product distribution. The introduction of water vapor enhances methanol selectivity by participating in methanol formation and facilitating its desorption from the catalyst surface (Fig. 2e), while increasing the discharge power can shift the dominant product from methanol to acetic acid when using Cu/Al_2O_3, which is not significant for the plasma only system (Fig. 2f and g).[75] These findings underscore the versatility of Cu-based catalysts in plasma-catalytic systems and highlight the importance of catalyst design and reaction conditions in steering the conversion of CH_4 and CO_2 toward desired oxygenates.
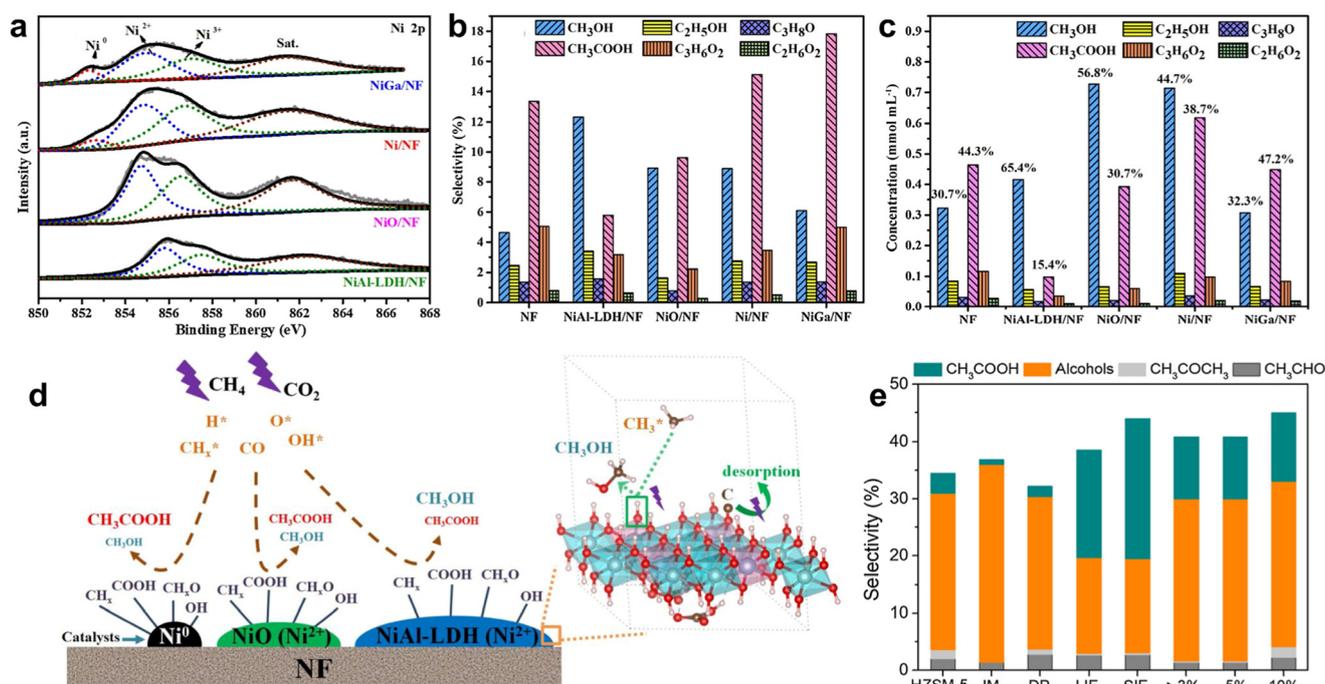

Fig. 3 (a) Ni 2p XPS spectra of NiAl-LDH/NF, NiO/NF, Ni/NF and NiGa/NF; (b) the selectivity of liquid products; (c) absolute concentration of the oxygenates; (d) the possible reaction pathways for the formation of liquid products on different catalysts via the plasma–catalytic approach.[43] Copyright 2023, Elsevier; (e) oxygenate generation from CH_4/CO_2 over Ni/HZSM-5 catalysts packed in the DBD reactor with Al foil as the ground electrode.[44] Copyright 2023, Springer Nature.

3.1.2 Ni-based catalysts. Ni-based catalysts have also demonstrated remarkable effectiveness in CO_2/CH_4 conversion to oxygenates, with their performance being significantly influenced by the chemical state of Ni species, support properties, and reactor configuration. These catalysts offer considerable tunability in the distribution of oxygenated products, enabling the rational adjustment of selectivity toward alcohols or acids through modulation of the Ni oxidation state.

Li et al. designed a series of structured Ni-foam (NF) supported catalysts to elucidate the role of Ni active sites.[43] As shown in Fig. 3a–c, the Ni^0 in Ni/NF and NiGa/NF catalysts showed high total liquid selectivity (>30%) with CH_3COOH as the dominant product (>15% selectivity). In contrast, the Ni^{2+} in NiO/NF yielded comparable selectivity for CH_3OH (8.9%) and CH_3COOH (9.6%). Surprisingly, NiAl-layered double hydroxide (LDH)/NF, rich in surface –OH groups, exhibited the highest CH_3OH selectivity (12.3%) and negligible carbon deposition. An "–OH reservoir" mechanism was proposed (Fig. 3d), where the abundant –OH groups on ultrathin LDH nanosheets readily react with CH_3^* radicals to form methanol, while the inferior electron affinity of the –OH rich surface for carbon atoms endows the catalyst with high coke resistance.

Catalyst preparation, loading amount, and reactor design strongly influence the performance of Ni catalysts. Fan et al. used the solid ion exchange method (SIE) to prepare Ni/HZSM-5 and achieved ~45% oxygenate selectivity (Fig. 3e).[44] High Ni loading promotes alcohol formation via stronger Lewis acid sites but suppresses acetic acid. In contrast, low Ni loading (1 wt%) with the liquid ion-exchange method (LIE) or SIE favors acetic acid due to abundant Brønsted acid sites and framework Ni^{2+}. Using an Al foil electrode instead of water cooling significantly enhances alcohol selectivity, likely due to differences in CO electronic states affecting alcohol vs. acetic acid formation.

3.1.3 Co-based catalysts. In plasma-catalytic conversion of CH_4 and CO_2, Co-based catalysts exhibit distinct catalytic properties, particularly in promoting the formation of liquid oxygenates and long-chain hydrocarbons. Unlike Cu and Ni catalysts, which primarily produce C_1–C_2 products, Co-based catalysts actively facilitate C–C coupling, leading to the formation of various long-chain carbon products such as C_5–C_8 oxygenates.
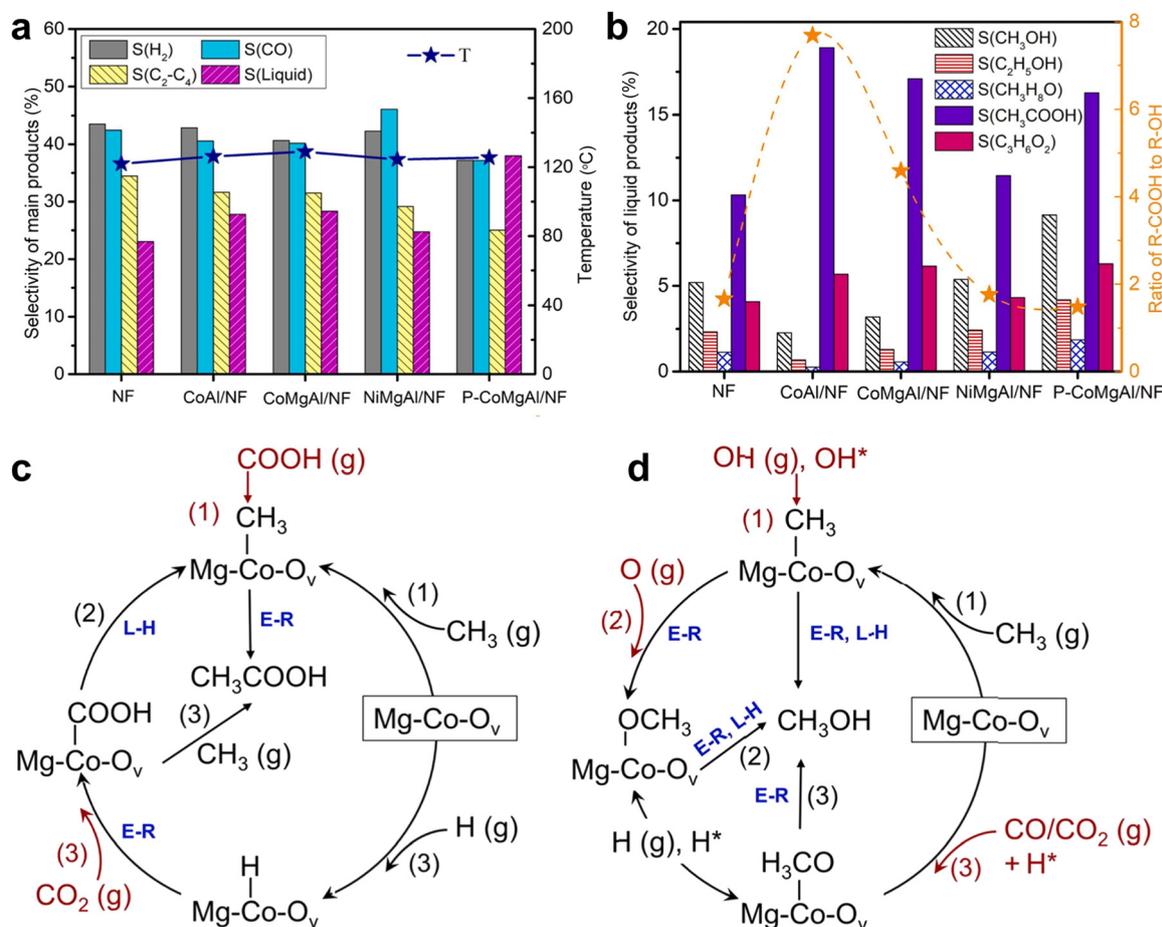

Fig. 4 (a) Overall selectivity for major products and (b) selectivity toward liquid oxygenates over different Co-based catalysts; the O_v-assisted reaction pathways (red arrows) for the formation of (c) CH_3COOH and (d) CH_3OH on Co-based catalysts.[31] Copyright 2022, Elsevier.

A key feature of Co catalysts is the complementary role played by metallic Co sites and oxygen vacancies (O_v) on the support. O_v in reducible oxides (*e.g.*, CeO_2, TiO_2) are well-known for activating CO_2 in thermal catalysis *via* electron donation. Under plasma, however, their role expands: O_v act as electron traps that stabilize anionic plasma intermediates such as CO_2^- or $\cdot CO_2^-$, which are otherwise short-lived in the gas phase. This stabilization enables subsequent hydrogenation or coupling reactions that bypass high-barrier thermal pathways. For example, Li *et al.* demonstrated that using Co/SiO_2 aerogel catalysts under ambient plasma conditions increased total liquid product selectivity to about 40%, with methanol and acetic acid as major products.[16] Traces of long-chain compounds such as C_6–C_7 hydrocarbons and esters were also detected, suggesting the intrinsic chain-growing ability on Co active sites. In subsequent work, Li *et al.* combined Co/SiO_2 with HZSM-5 zeolite in a composite bed, which further enhanced the formation of C_5–C_8 products including heptane, pentanol, and C_6 esters, highlighting the synergy between Co-mediated C–C coupling and zeolite-assisted oligomerization.[76]

Further insight into the Co–support interaction was provided by Dou *et al.*, who designed a Co–MgAlO–O_v structured catalyst.[31] The catalyst delivers a total oxygenate selectivity of 40%, attributed to the synergistic effect between O_v in MgAlO supports and the small size of Co nanoparticles

(Fig. 4a). Moreover, distinct distributions of liquid products are observed across different Co-based catalysts (Fig. 4b). Through combined experimental and computational studies, they identified metallic Co as the main site for acetic acid formation, where it strongly adsorbs CH_3 and COOH radicals, enabling coupling *via* a low-barrier E–R mechanism (Fig. 4c). In contrast, O_v on the MgAlO support preferentially captured CO_2 and oxygenated radicals (*e.g.*, O and OH), shifting the product towards methanol with a selectivity of ~9% (Fig. 4d). This bifunctional mechanism allows product distribution to be tuned by tailoring the catalyst's surface composition.

3.1.4 Other metal-based catalysts. Besides the Cu-, Ni-, and Co-based catalysts, other transition metal and noble metal-based catalysts are also investigated in plasma-catalytic CO_2/CH_4 conversion, such as Fe, Au, Ag, and Pt.[42,49,50,77] Fe-based catalysts, such as Fe–SiO_2 or carbon-embedded Fe/C-SiO_2, can promote the formation of valuable liquid oxygenates (such as acetic acid and longer-chain acids and alcohols) and control the composition of gaseous products.[42,47,76] Wang *et al.* reported that iron carbide phases (*e.g.*, ε-$Fe_{2.2}C$) facilitate CO_2 activation through surface defects, which weaken C–O bonds and enhance CO_2 conversion (Fig. 5a).[42] Additionally, Fe sites promote the adsorption and activation of CH_4 and plasma-generated radicals, leading to higher selectivity toward C_{2+} hydrocarbons and oxygenates (Fig. 5a and b). Introduction of K further enhances the performance by moderating H_2
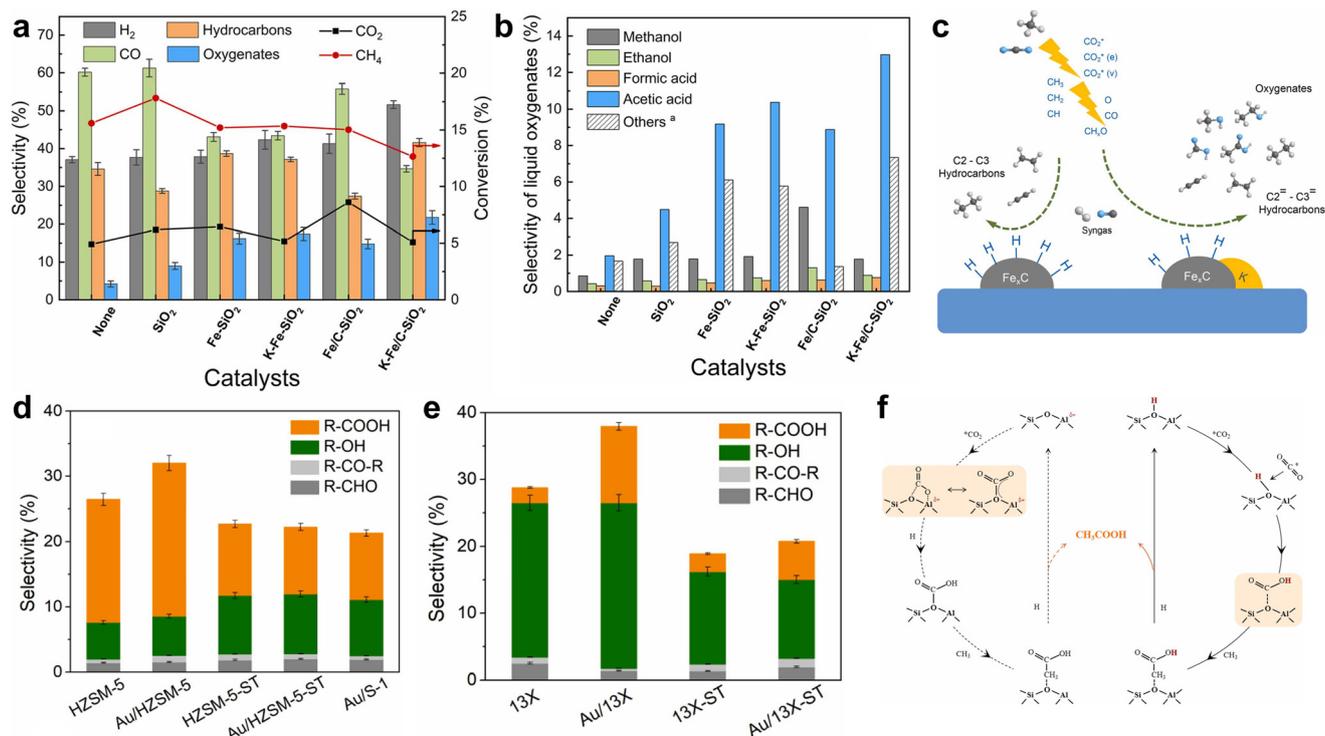

Fig. 5 (a) Selectivity to gaseous hydrocarbons and (b) selectivity to liquid oxygenates over different Fe-based catalysts; (c) reaction mechanisms proposed for plasma-catalytic conversion of CO_2 and CH_4.[42] Copyright 2023, Elsevier; selectivity to liquid oxygenates for (d) Au/HZSM-5, HZSM-5-ST, Au/HZSM-5-ST and Au/S-1 catalysts, and (e) 13X, Au/13X, 13X-ST and Au/13X-ST in plasma-catalytic CH_4/CO_2 conversion; (f) reaction pathways for acetic acid formation over BAS in plasma-catalytic CH_4/CO_2 conversion on HZSM-5 zeolite.[50] Copyright 2024, Elsevier.

adsorption, increasing the unsaturated/saturated hydrocarbon ratio to ~1 and promoting long-chain oxygenate production (Fig. 5c). The K-Fe/C-SiO$_2$ catalyst maintains excellent stability over 9 hours, highlighting superior coke resistance for promoted catalysts. In another work, Fe/SiO$_2$ aerogels achieve ~40% total liquid selectivity, where the mesoporous SiO$_2$ support stabilizes CH$_x$O intermediates against CO decomposition.[16] Composite beds with HZSM-5 enable product tuning: CH$_4$-rich conditions favor acetic acid (~26%), while CO$_2$-rich conditions favour methanol (~24%), demonstrating the synergistic effect of Fe active sites and acid sites on HZSM-5 supports.[76]

Au-based catalysts present unique catalytic effects towards higher selectivity for acetic acid. Wang *et al.* designed a series of Au-zeolite catalysts to elucidate the role of Au species and acid sites.[50] The Au/HZSM-5 catalyst, containing both Au^{3+} and BAS, exhibited the highest selectivity toward CH$_3$COOH (Fig. 5d). In contrast, Au/HZSM-5-ST, which lost both BAS and Au^{3+} after steam treatment, showed a dramatic decrease in acetic acid selectivity and a shift toward alcohols. Similarly, Au/13X, with only Lewis acid sites (LAS) and a small amount of Au^{3+}, still favors R-OH production, though the presence of Au^{3+} slightly enhanced acetic acid formation (Fig. 5e). A "Au^{3+}-BAS synergy" mechanism was proposed, where Au^{3+} species located in the H$^+$ sites of HZSM-5 enhance CO$_2$ activation and facilitate the bicarbonate pathway toward acetic acid, while the poor dispersion and low loading of Au limit its overall catalytic activity in the plasma environment (Fig. 5f).

3.2 Support

In plasma-catalytic CO$_2$/CH$_4$ conversion, the support plays a far more active role than merely serving as a high-surface-area scaffold for metal dispersion. It critically modulates the local electric field, influences discharge characteristics (*e.g.*, microdischarge density and electron energy distribution), and directly participates in surface reactions through its chemical functionality. This role fundamentally distinguishes it from supports in conventional thermal catalysis. Unlike thermal catalyst supports, which are primarily designed for thermodynamic stability and active site dispersion, supports for plasma catalysis must also actively manipulate the non-equilibrium plasma environment (*e.g.*, by modulating local electric fields and mediating surface charge interactions) and demonstrate stability against plasma-specific challenges such as physical etching and charge accumulation, rather than solely against thermal sintering or chemical poisoning. An ideal support must therefore combine a high specific surface area, appropriate acid–base properties, robust thermal and plasma stability, and strong metal–support interactions to maximize the synergy between plasma physics and catalytic chemistry.

This synergy is exemplified by BAS in zeolitic supports such as HZSM-5, whose function diverges markedly between thermal and plasma environments. In conventional thermal catalysis, BAS protonates olefins to form carbenium-like intermediates that drive C–C coupling. Under NTP conditions, however, olefins are scarce; instead, BAS act as proton donors to plasma-generated anionic species such as CO$_2^-$ or ·CO$_2^-$, yielding bicarbonate-like surface intermediates.[50] These species readily undergo radical-surface reactions with gas-phase ·CH$_3$ to form oxygenates like acetic acid or ethanol. Consequently, the "acidity" that matters in plasma catalysis is not oriented toward carbocation stabilization, but rather toward facilitating proton transfer to and stabilization of charged plasma-generated intermediates. This paradigm shift underscores that support design in plasma catalysis must be guided by plasma-specific reaction mechanisms, not thermal analogues.

The physical properties of the support significantly affect the plasma environment. The dielectric constant (ε_r) primarily determines the discharge behavior. Materials such as BaTiO$_3$ with a high ε_r act as macroscopic dipoles, which enhances the local field and the formation of intense micro-discharges. Mei *et al.* found that BaTiO$_3$ beads could double the average electric field and mean electron energy of the CO$_2$ discharge (Fig. 6a and b), thus boosting CO$_2$-to-CO conversion (Fig. 6c).[78] Conversely, the support (*e.g.*, SiO$_2$, Al$_2$O$_3$) with low-ε_r induces a weaker polarization effect, leading to a more diffuse and uniform discharge (*e.g.*, glow-like), which can be beneficial for uniform surface reactions. Furthermore, porous supports such as zeolites and MOFs exhibit nano-confinement effects.[79] By extending the residence time of active species within pores, secondary reactions can be promoted. For example, ZSM-5 zeolite can enhance the selectivity of CH$_4$ conversion to C$_2$ hydrocarbons *via* CH$_x$ intermediate coupling.[80]

Tailoring the electronic structure of metals is a primary function of supports, which directly governs reaction pathways and product selectivity. This is well-illustrated by Cu-based catalysts in the plasma-driven conversion of CO$_2$/CH$_4$. Basic supports like Al(OH)$_3$ and Mg(OH)$_2$ enhance the formation of Cu^{2+} species, directing the reaction toward production of methanol and other alcohols (Fig. 2a).[73] In contrast, the HZSM-5 zeolite support can stabilize Cu$^+$ species and provides Brønsted acid sites, thus facilitating CO$_2$ protonation and C–C coupling. This synergistic effect contributes to higher selectivity toward C$_2$ oxygenates, such as acetic acid. Meanwhile, a balanced Cu^{2+}/Cu$^+$ ratio was observed when dispersed on neutral supports such as SiO$_2$ and TiO$_2$, contributing to both alcohol and acid formation with moderate selectivity.

Furthermore, the surface acidity or basicity of the support critically influences the CO$_2$/CH$_4$ adsorption and activation. Qi *et al.* used UiO-66-NH$_2$ as a support for Cu in plasma-catalytic CO$_2$/CH$_4$ conversion. Th synergistic effect of Cu and UiO-66-NH$_2$ realizes an overall liquid product selectivity of 53.4%, with 60.8% C$_{2+}$ oxygenates in the liquid products (Fig. 6d). The UiO-66-NH$_2$ support with a high surface area and porosity offers abundant adsorption sites, while its –NH$_2$
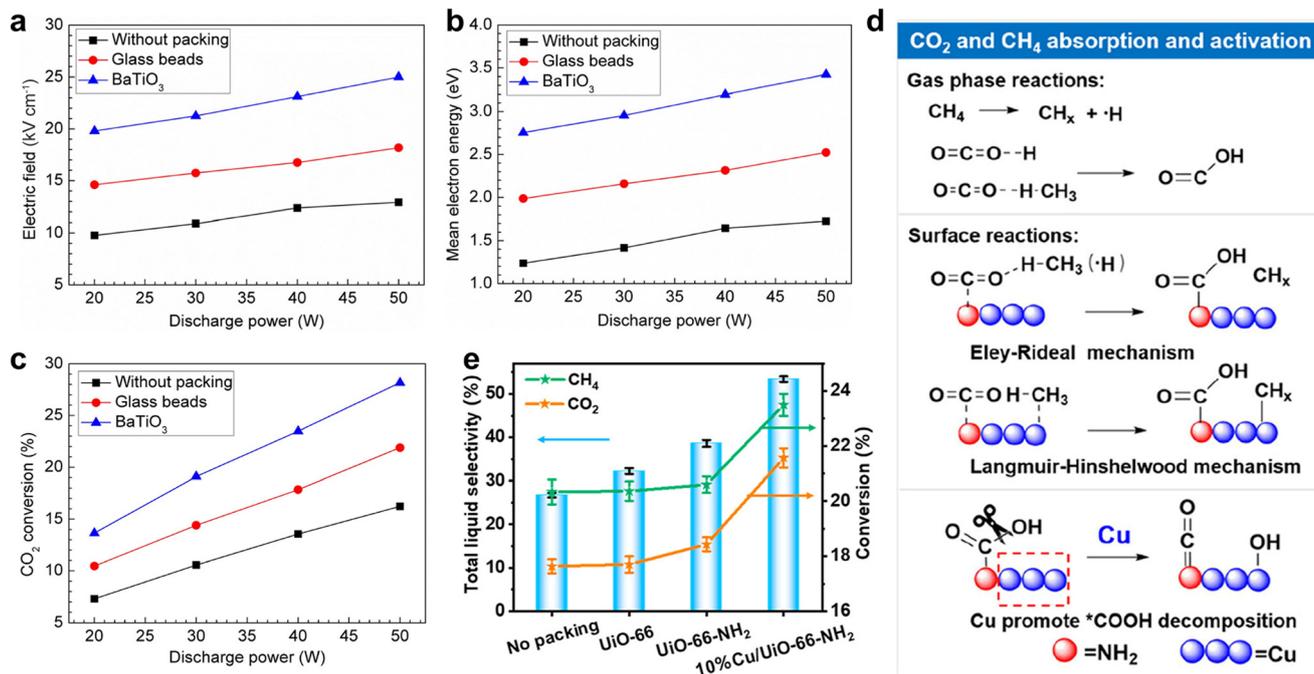
Fig. 6 Effect of packing materials (*i.e.* glass beads and $BaTiO_3$) on (a) average electric field strength, (b) mean electron energy, and (c) CO_2 conversion in the CO_2 DBD at different discharge powers.[78] Copyright 2014, IOP Publishing; (d) gas conversion and total liquid selectivity for different catalysts in CO_2/CH_4 conversion; (e) proposed mechanism for absorption and activation of CO_2 and CH_4, and the role of Cu in enhancing *COOH conversion.[48] Copyright 2024, American Chemical Society.

groups serve as Lewis basic sites that enhance CO_2 chemisorption and promote *COOH intermediate formation (Fig. 6e). The organic framework can also facilitate CH_4 activation to obtain stable *CH_3 and *CH_2 species. Strong electronic interaction with Cu further promotes C–H and C=O bond cleavage, accelerating the conversion of *COOH into *CO and other intermediates.

4 Reactor optimization

DBD,[81] microwave discharge,[82] gliding arc discharge,[83] and corona discharge[84] reactors are common types of plasma reactors. Among these, the DBD reactor is widely applied in plasma catalytic conversion due to its simple structure and flexible operating conditions.[15,75,85] However, traditional DBD reactors suffer from inherent limitations, such as unfavorable reaction conditions for multiple components, uneven discharge distribution, and unavoidable decomposition of products within the plasma discharge zone.[15,86,87] Consequently, a series of improvement strategies have been proposed, focusing on reactor structure design, electrode structure design, and reactor configurations to promote the CH_4 and CO_2 conversion.

4.1 Reactor structure design

A primary challenge in conventional DBD systems lies in their basic flow and reaction zone design. Conventional DBD reactors typically employ a simple parallel or coaxial structure, characterized by a basic zoned layout with a single

inlet and outlet, which is not conducive to multi-component reactions. Uytdenhouwen *et al.*[87] developed a novel multi-inlet/outlet parallel-plate DBD reactor to optimize DRM by strategically altering gas flow and mixing patterns (Fig. 7a). Their key innovation lies in moving beyond the conventional "one inlet-one outlet" design to spatially and temporally control reactant introduction. This configuration prevents the kinetic imbalance often seen in conventional reactors, where one reactant (*e.g.*, CH_4) is over-converted while the other (*e.g.*, CO_2) remains under-converted, thereby maintaining locally favourable CO_2/CH_4 ratios along the reaction path. As a result, they achieved significant enhancement in total conversion up to 19.2%, compared to 13.7% in the benchmark configuration. With the same total specific energy input (SEI), due to the improved gas conversion, the overall energy cost was effectively reduced, obtaining a benchmark value of 1.63 kWh mol^{-1}. Additionally, they demonstrated that altering the gas flow direction to reduce velocity, while keeping residence time constant, further improved performance, highlighting the critical role of reactor geometry and flow dynamics in plasma-assisted chemical conversion.

4.2 Electrode structure design

The operation of the DBD reactor is characterized by the breakdown of the gas gap, leading to the formation of numerous filamentary micro-discharges. These transient current channels are distributed randomly and exhibit
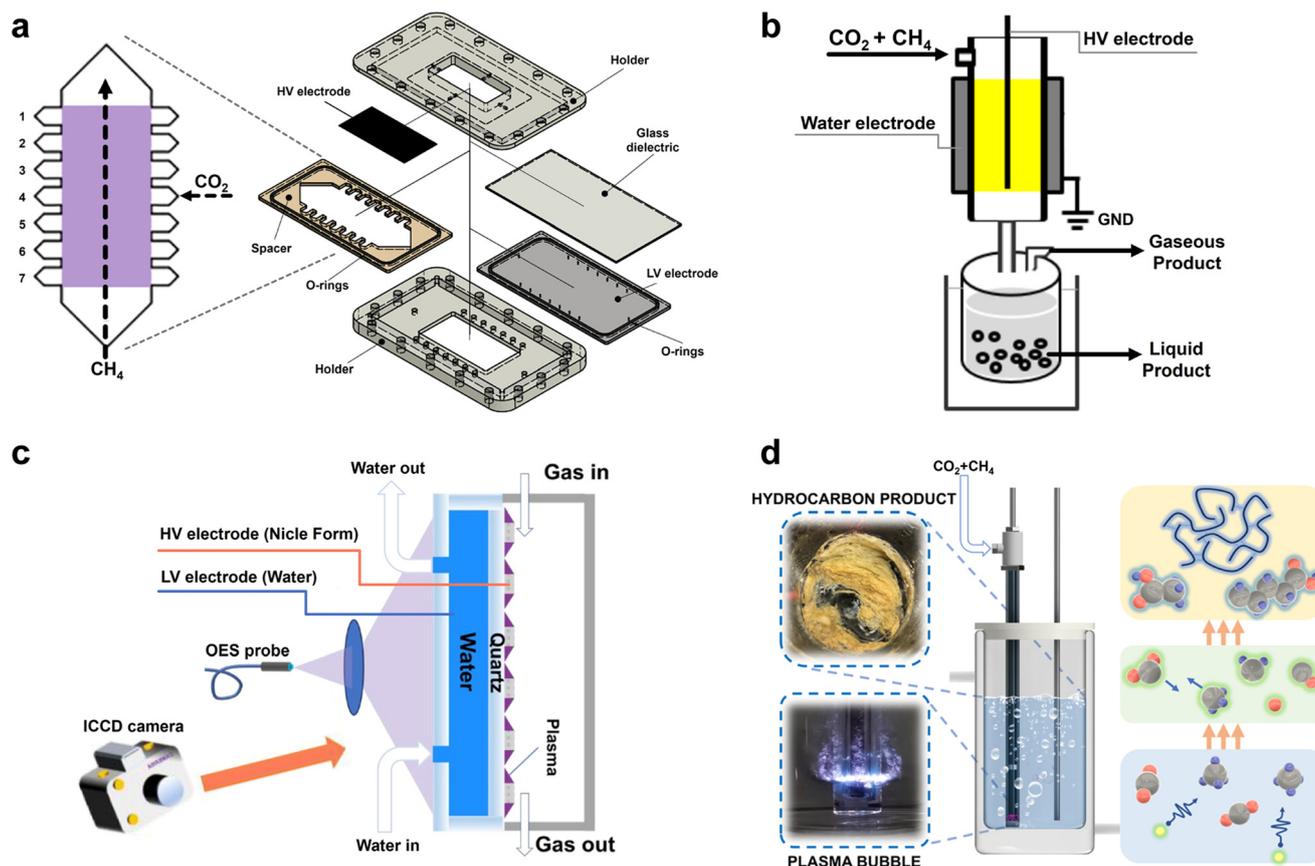
Fig. 7 (a) Expanded view of a parallel plate DBD reactor.[87] Copyright 2021, Elsevier; (b) design of a water electrode as the ground electrode in the DBD reactor.[15] Copyright 2017, Wiley-VCH; (c) water-electrode surface microdischarge (SMD) reactor using nickel foam as the high-voltage electrode.[88] Copyright 2025, Elsevier; (d) plasma bubble reactor configuration.[19] Copyright 2024, American Chemical Society.

significant spatial non-uniformity, a behavior attributed to the intrinsic stochasticity of the discharge initiation process. To enhance discharge uniformity a water electrode is employed as the ground electrode in the DBD reactor.[81,89] Water conductivity is a critical parameter in water-electrode plasma systems, directly governing electric field distribution, plasma ignition, energy coupling efficiency, and discharge stability.[90,91] Operationally, low-conductivity deionized water enables clean discharges but requires higher ignition voltages; medium-conductivity water (e.g., tap water) offers easier ignition with potential impurity issues, while high-conductivity solutions improve impedance matching and species yield at the risk of side reactions and corrosion. Thus, water selection involves balancing generation efficiency, stability, and application goals.

Wang et al. designed an innovative electrode structure as shown in Fig. 7b.[15] They realized the one-step reforming of CO_2 and CH_4 into liquid fuels and chemicals, such as acetic acid, methanol, and ethanol, at room temperature and atmospheric pressure, achieving a total oxygenate selectivity of 50–60%, with acetic acid selectivity reaching 40%. Notably, the synthesis of acetic acid from CO_2 and CH_4 proceeded with 100% atom economy, a reaction considered thermodynamically unfavorable and nearly unattainable via

conventional thermal catalysis. The water electrode enhances energy efficiency through a dual functionality: it promotes uniform plasma discharge via superior charge dissipation and electric field redistribution, and effectively removes joule heat to maintain near-ambient reaction temperatures. This combination not only suppresses energy-wasting parasitic reactions (e.g., total oxidation or cracking) but also stabilizes key reactive intermediates (such as $\cdot CH_3$ and $\cdot COOH$), thereby steering electron-driven chemistry toward selective oxygenate formation. By simultaneously optimizing plasma homogeneity and thermal management, the water electrode outperforms conventional solid metal electrodes as a strategic enabler of energy-efficient CO_2/CH_4 valorization.

In conventional DBD reactors, the plasma region typically spans the entire discharge gap, which tends to cause re-decomposition of generated products, resulting in low conversion efficiency. To address this, Feng et al.[88] developed a novel surface microdischarge (SMD) reactor utilizing metal-loaded nickel foam (NF) as the high-voltage electrode (Fig. 7c). By spatially confining the plasma to the dielectric surface, this design enables synthesized NH_3 to rapidly diffuse through the porous NF electrode into a plasma-free "product-safe zone", effectively suppressing energy-wasting reverse reactions. This strategic separation of reaction and

product zones directly translates into superior energy efficiency: under identical conditions (SEI = 10 kJ L^{-1}), the SMD system with Ni–Co/NF achieved an NH_3 energy yield of 0.79 g kWh^{-1}, a 38.6% improvement over the plasma-only baseline (0.57 g kWh^{-1}). Thus, the SMD electrode architecture not only preserves products but also significantly enhances the fraction of electrical energy channeled into useful chemical output.

4.3 Reactor configuration

Although structural optimization of DBD reactors can enhance reaction performance, DBD reactors are typically limited to synthesizing simple small-molecule products, such as methanol, formic acid, ethanol, and acetic acid. The high-energy environment of the plasma zone often favors the formation of these simpler compounds over more complex hydrocarbons. To overcome the limitation in producing long-chain hydrocarbons, Knezevic et al.[19] employed a plasma bubble reactor that directly initiates discharge at the interface of CO_2/CH_4 gas bubbles and water at atmospheric pressure and room temperature (Fig. 7d). This configuration successfully produced solid long-chain hydrocarbons (up to C_{40}) when the CO_2 content in the feed gas was below 40%, alongside the co-production of syngas and liquid-phase oxygenates such as alcohols and acids. This work breaks the previous constraint of the DBD reactor predominantly yielding short-chain products and, for the first time, demonstrates the feasibility of synthesizing long-chain hydrocarbons under mild conditions. Nevertheless, challenges remain for this plasma bubble reactor, particularly in effectively coupling plasma-generated products with catalysts to further control product selectivity.

4.4 Thin-film electrodes

In addition to packing particulate catalysts inside plasma reactors, depositing catalysts directly as thin films on electrode surfaces represents another effective strategy. The reduced thickness shortens the transport distance for short-lived plasma species, thereby improving their utilization at the catalyst surface. Porous thin-film structures also provide a large plasma-exposed surface area, enhancing active-site accessibility and promoting surface-dominated reaction pathways. When combined with helical electrodes, thin-film configurations can generate surface-confined plasmas directly on and within the catalyst layer, strengthening plasma-catalyst synergy and minimizing the energy losses typical of post-plasma catalytic systems.[33,92]

Gregory and co-workers developed an Ir/TiO_2 thin-film electrode for plasma-assisted CO_2 hydrogenation to CH_4, demonstrating that the thin-film structure not only stabilized the plasma discharge but also promoted CO_2 activation and hydrogenation on Ir sites, achieving superior methane selectivity and energy efficiency compared with particulate catalysts.[93] Specifically, this configuration delivered a fuel production efficiency of 3.5%, a key metric of energy

utilization, and exhibited a CH_4 formation rate two orders of magnitude higher per unit catalyst mass than conventional packed-bed systems. The enhancement stems from the intimate coupling between plasma and the catalyst: by confining the discharge directly over the ultrathin catalytic layer (<2 μm), reactive species (e.g., ·H) are generated in immediate proximity to active Ir sites, minimizing transport losses and avoiding energy-wasting gas-phase side reactions. Moreover, the separation of H_2 dissociation (driven by plasma) and CO_2 hydrogenation (catalyzed by Ir) reduces the overall energy demand, as the catalyst bypasses the need for plasma-mediated H_2 activation. Similarly, in CO_2–CH_4 co-conversion systems, thin-film electrodes based on Cu, Ni, or Co are expected to leverage intensified local electric fields and directed intermediate transport to enhance the formation of oxygenated products.[92,94] Thin-film electrodes are particularly compatible with microdischarge or surface-discharge reactors, which help suppress decomposition of gas products and provide model platforms for mechanistic studies of plasma-catalyst synergy.

5 Conclusions and outlook

NTP represents a promising and sustainable approach for catalytic conversion of CO_2/CH_4 into value-added oxygenates. This mini-review has summarized the recent advances in the plasma-catalytic conversion of CO_2 and CH_4 into value-added oxygenates from supported catalyst design and plasma reactor design. For supported catalysts, the metal active sites (e.g., Cu, Ni, Co, Fe, Au) and their properties, such as valence state, particle size, and dispersion, play a primary role in determining the reaction pathway, while the support further enhances product selectivity and activity through its interaction with both the metals and plasma. For plasma reactors, reactor structure, and electrode structure, reactor configuration fundamentally determines the efficiency and pathways of plasma reactions.

A central finding is that catalyst design for plasma environments must move beyond thermal catalysis paradigms. As discussed in sections 2 and 3, the optimal active sites (e.g., Cu^{2+} for alcohols, Cu^+ for acids) and support functions (e.g., Brønsted acid sites for protonating plasma-generated anions) are defined by their ability to capture and steer transient plasma-generated species (radicals, ions, vibrationally excited molecules) rather than just activate stable reactants. Furthermore, energy efficiency remains a paramount challenge. As analyzed in section 4, while innovative reactor designs (e.g., water electrodes, surface microdischarges) can enhance efficiency by improving discharge uniformity and creating product-safe zones, the energy cost of breaking stable C–H and C=O bonds via electron impact is still high. Critically, overcoming the energy efficiency bottleneck requires reactor architectures that not only localize energy input to targeted molecular activation but also maximize plasma-catalyst synergy while minimizing all parasitic energy losses, including those from gas heating,

non-productive electron scattering, and unintended side reactions.

Therefore, future research should pursue integrated strategies that co-optimize catalysts and reactors to address both selectivity and energy efficiency. Three grounded directions emerge from the present analysis:

(1) Rational catalyst design for enhancing conversion and selectivity. Future catalysts should be engineered to directly leverage the non-equilibrium energy carriers in plasma. This involves designing "vibrationally-coupled" catalysts (*e.g.*, using oxides like ZrO_2 or CeO_2 with tailored phonon spectra) that can resonantly accept energy from plasma-generated vibrationally excited CO_2 ($CO_2(v)$), a key species discussed in section 2.3.3. This resonant energy transfer could promote surface reactions at lower overall energy input, moving beyond reliance on high-energy electron collisions alone. Furthermore, elevating the C_{2+} product selectivity is essential for synthesis of high-value chemicals. It's necessary to design catalysts with spatially organized bifunctional sites that can co-adsorb and orient key intermediates for selective C–C coupling. For instance, the catalyst surface with adjacent metallic sites (*e.g.*, Co, Fe) and acidic sites (*e.g.*, HZSM-5) is promising for synergistically adsorbing ·CH_3 radicals and activating CO_2 into ·COOH, facilitating acetic acid formation *via* a low-barrier E–R mechanism.

(2) Reactor optimization should prioritize energy localization, intensified mass transfer, and product preservation. Building on the design principles outlined in section 4, a promising path forward is the development of "zoned synergistic plasma reactors". In this advanced configuration, CO_2 and CH_4 activation are decoupled and individually optimized in separate plasma zones (*e.g.*, microwave for CO_2, DBD for CH_4), with the generated reactive intermediates then channeled into a common catalytic zone for selective conversion. This approach enhances energy efficiency by matching each molecule's activation profile to the most suitable plasma source, while also improving overall process control. Furthermore, reactor architecture must be closely integrated with catalyst design. Practical strategies include directly coating catalysts on electrodes (section 4.4), fabricating 3D-printed structured electrodes, and using ordered high-dielectric fillers (*e.g.*, $BaTiO_3$ monoliths) to replace random particle packings.

(3) To elucidate the complex mechanisms in plasma catalysis, future research should integrate advanced *in situ* diagnostics (*e.g.*, OES, LIF, DRIFTS) with isotopically labelled experiments and targeted probing. Coupling these experimental insights with multiscale theoretical simulations, from DFT to kinetic modelling, is essential. This synergistic approach will enable the unambiguous identification of transient species, disentangle reaction pathways, and distinguish chemical effects from physical transport, thereby advancing the fundamental understanding and rational design of plasma-catalytic processes.

Conflicts of interest

The authors declare no conflict of interest.

Data availability

No primary research results, software or code have been included and no new data were generated or analysed as part of this review.

Supplementary information (SI) is available. See DOI: https://doi.org/10.1039/d5im00347d.

Acknowledgements

References

1 C. Hepburn, E. Adlen, J. Beddington, E. A. Carter, S. Fuss, N. Mac Dowell, J. C. Minx, P. Smith and C. K. Williams, The technological and economic prospects for CO_2 utilization and removal, *Nature*, 2019, **575**, 87–97.

2 X. Meng, X. Cui, N. P. Rajan, L. Yu, D. Deng and X. Bao, Direct methane conversion under mild condition by thermo-, electro-, or photocatalysis, *Chem*, 2019, **5**, 2296–2325.

3 R. W. Howarth, A. Ingraffea and T. Engelder, Should fracking stop?, *Nature*, 2011, **477**, 271–275.

4 A. Rode, T. Carleton, M. Delgado, M. Greenstone, T. Houser, S. Hsiang, A. Hultgren, A. Jina, R. E. Kopp, K. E. McCusker, I. Nath, J. Rising and J. Yuan, Estimating a social cost of carbon for global energy consumption, *Nature*, 2021, **598**, 308–314.

5 X. Tao, M. Bai, X. Li, H. Long, S. Shang, Y. Yin and X. Dai, CH_4-CO_2 reforming by plasma-challenges and opportunities, *Prog. Energy Combust. Sci.*, 2011, **37**, 113–124.

6 M. M. Zain and A. R. Mohamed, An overview on conversion technologies to produce value added products from CH_4 and CO_2 as major biogas constituents, *Renewable Sustainable Energy Rev.*, 2018, **98**, 56–63.

7 F. Cheng, X. Duan and K. Xie, Dry reforming of CH_4/CO_2 by stable Ni nanocrystals on porous single-crystalline MgO monoliths at reduced temperature, *Angew. Chem., Int. Ed.*, 2021, **60**, 18792–18799.

8 H. Wang, G. Cui, H. Lu, Z. Li, L. Wang, H. Meng, J. Li, H. Yan, Y. Yang and M. Wei, Facilitating the dry reforming of methane with interfacial synergistic catalysis in an $Ir@CeO_{2-x}$ catalyst, *Nat. Commun.*, 2024, **15**, 3765.

9 J. Bao, G. Yang, Y. Yoneyama and N. Tsubaki, Significant advances in C1 catalysis: Highly efficient catalysts and catalytic reactions, *ACS Catal.*, 2019, **9**, 3026–3053.

10 Y. J. Zhou, E. J. Kerkhoven and J. Nielsen, Barriers and opportunities in bio-based production of hydrocarbons, *Nat. Energy*, 2018, **3**, 925–935.

11 X. Li, C. Wang and J. Tang, Methane transformation by photocatalysis, *Nat. Rev. Mater.*, 2022, **7**, 617–632.

12 F. O. Ochedi, D. Liu, J. Yu, A. Hussain and Y. Liu, Photocatalytic, electrocatalytic and photoelectrocatalytic conversion of carbon dioxide: A review, *Environ. Chem. Lett.*, 2021, **19**, 941–967.

13 D. Wakerley, S. Lamaison, J. Wicks, A. Clemens, J. Feaster, D. Corral, S. A. Jaffer, A. Sarkar, M. Fontecave, E. B. Duoss, S. Baker, E. H. Sargent, T. F. Jaramillo and C. Hahn, Gas diffusion electrodes, reactor designs and key metrics of low-temperature CO_2 electrolysers, *Nat. Energy*, 2022, **7**, 130–143.

14 C. Kim, J. Lee, S. Lee, W. Jung, H. Min, J. Choi, S. Kim, Y. T. Kim, J. Lee, J. S. Yoo and J. H. Moon, High-selectivity room-temperature partial oxidation of methane to methanol enabled by electrochemical oxygen promotion on IrO_2 catalysts, *Nat. Catal.*, 2025, **8**, 688–696.

15 L. Wang, Y. Yi, C. Wu, H. Guo and X. Tu, One-step reforming of CO_2 and CH_4 into high-value liquid chemicals and fuels at room temperature by plasma-driven catalysis, *Angew. Chem., Int. Ed.*, 2017, **56**, 13679–13683.

16 D. Li, V. Rohani, F. Fabry, A. Parakkulam Ramaswamy, M. Sennour and L. Fulcheri, Direct conversion of CO_2 and CH_4 into liquid chemicals by plasma-catalysis, *Appl. Catal., B*, 2020, **261**, 118228.

17 P. Chawdhury, Y. Wang, D. Ray, S. Mathieu, N. Wang, J. Harding, F. Bin, X. Tu and C. Subrahmanyam, A promising plasma-catalytic approach towards single-step methane conversion to oxygenates at room temperature, *Appl. Catal., B*, 2021, **284**, 119735.

18 J. Sun, Z. Qu, Y. Gao, T. Li, J. Hong, T. Zhang, R. Zhou, D. Liu, X. Tu, G. Chen, V. Brüser, K.-D. Weltmann, D. Mei, Z. Fang, A. Borras, A. Barranco, S. Xu, C. Ma, S. Dou, S. Zhang, T. Shao, G. Chen, D. Liu, X. Lu, Z. Bo, W.-H. Chiang, K. Vasilev, M. Keidar, A. Nikiforov, A. R. Jalili, P. J. Cullen, L. Dai, V. Hessel, A. Bogaerts, A. B. Murphy, R. Zhou and K. Ostrikov, Plasma power-to-X (PP2X): Status and opportunities for non-thermal plasma technologies, *J. Phys. D: Appl. Phys.*, 2024, **57**, 503002.

19 J. Knezevic, T. Zhang, R. Zhou, J. Hong, R. Zhou, C. Barnett, Q. Song, Y. Gao, W. Xu, D. Liu, N. Proschogo, B. Mohanty, J. Strachan, B. Soltani, F. Li, T. Maschmeyer, E. C. Lovell and P. J. Cullen, Long-chain hydrocarbons from nonthermal plasma-driven biogas upcycling, *J. Am. Chem. Soc.*, 2024, **146**, 12601–12608.

20 J. Feng, X. Sun, Z. Li, X. Hao, M. Fan, P. Ning and K. Li, Plasma-assisted reforming of methane, *Adv. Sci.*, 2022, **9**, e2203221.

21 G. Scarduelli, G. Guella, D. Ascenzi and P. Tosi, Synthesis of liquid organic compounds from CH_4 and CO_2 in a dielectric barrier discharge operating at atmospheric pressure, *Plasma Processes Polym.*, 2011, **8**, 25–31.

22 J. Sentek, K. Krawczyk, M. Młotek, M. Kalczewska, T. Kroker, T. Kolb, A. Schenk, K.-H. Gericke and K. Schmidt-Szałowski, Plasma-catalytic methane conversion with carbon dioxide in dielectric barrier discharges, *Appl. Catal., B*, 2010, **94**, 19–26.

23 V. Rosa, F. Cameli, G. D. Stefanidis and K. M. Van Geem, Integrating materials in non-thermal plasma reactors: Challenges and opportunities, *Acc. Mater. Res.*, 2024, **5**, 1024–1035.

24 R. Snoeckx and A. Bogaerts, Plasma technology-a novel solution for CO_2 conversion?, *Chem. Soc. Rev.*, 2017, **46**, 5805–5863.

25 M. R. Ahasan, M. M. Hossain and R. Wang, Dielectric barrier discharge reactors for plasma-assisted CO_2 and CH_4 conversion: A comprehensive review of reactor design, performance, and future prospects, *Energy Technol.*, 2025, **13**, 2401177.

26 S. Liu, L. R. Winter and J. G. Chen, Review of plasma-assisted catalysis for selective generation of oxygenates from CO_2 and CH_4, *ACS Catal.*, 2020, **10**, 2855–2871.

27 A. Bogaerts, G. Centi, V. Hessel and E. Rebrov, Challenges in unconventional catalysis, *Catal. Today*, 2023, **420**, 114180.

28 P. Lamichhane, N. Pourali, L. Scott, N. N. Tran, L. Lin, M. E. Gelonch, E. V. Rebrov and V. Hessel, Critical review:'Green'ethylene production through emerging technologies, with a focus on plasma catalysis, *Renewable Sustainable Energy Rev.*, 2024, **189**, 114044.

29 R. S. Abiev, D. A. Sladkovskiy, K. V. Semikin, D. Y. Murzin and E. V. Rebrov, Non-thermal plasma for process and energy intensification in dry reforming of methane, *Catalysts*, 2020, **10**, 1358.

30 V. Maslova, R. Nastase, G. Veryasov, N. Nesterenko, E. Fourré and C. Batiot-Dupeyrat, Current status and challenges of plasma and plasma-catalysis for methane coupling: A review, *Prog. Energy Combust. Sci.*, 2024, **101**, 101096.

31 L. Dou, L. Liu, Y. Gao, J. Li, X. Hu, S. Zhang, K. Ostrikov and T. Shao, Disentangling metallic cobalt sites and oxygen vacancy effects in synergistic plasma-catalytic CO_2/CH_4 conversion into oxygenates, *Appl. Catal., B*, 2022, **318**, 121830.

32 J. Tornin, C. Labay, F. Tampieri, M.-P. Ginebra and C. Canal, Evaluation of the effects of cold atmospheric plasma and plasma-treated liquids in cancer cell cultures, *Nat. Protoc.*, 2021, **16**, 2826–2850.

33 T. Nozaki, X. Chen, D.-Y. Kim and C. Zhan, Combination of DBD and catalysts for CH_4 and CO_2 conversion: Basics and applications, *Plasma Chem. Plasma Process.*, 2023, **43**, 1385–1410.

34 S. K. Dhali, Plasma chemistry and applications of atmospheric pressure transient electrical discharges, in *Emerging Applications of Ions and Plasmas*, Springer, 2025, pp. 267–296.

35 T. Butterworth, A. Van de Steeg, D. Van den Bekerom, T. Minea, T. Righart, Q. Ong and G. Van Rooij, Plasma induced vibrational excitation of CH_4-a window to its mode selective processing, *Plasma Sources Sci. Technol.*, 2020, **29**, 095007.

36 A. Van de Steeg, T. Butterworth, D. Van den Bekerom, A. Silva, M. Van de Sanden and G. Van Rooij, Plasma activation of N_2, CH_4 and CO_2: an assessment of the vibrational non-equilibrium time window, *Plasma Sources Sci. Technol.*, 2020, **29**, 115001.

37 J. Sun, Q. Chen, W. Qin, H. Wu, B. Liu, S. Li and A. Bogaerts, Plasma-catalytic dry reforming of CH_4: Effects of plasma-generated species on the surface chemistry, *Chem. Eng. J.*, 2024, **498**, 155847.

38 K. H. Rouwenhorstm and L. Lefferts, Plasma-catalytic ammonia synthesis via eley-rideal reactions: A kinetic analysis, *ChemCatChem*, 2023, **15**, e202300078.

39 R. Y. A. Mohamed, R. K. Kumarachari, S. P. N. Bukke, D. Neerugatti, Y. T. Mekasha and K. Bandarapalle, Plasma catalysis for sustainable industry: lab-scale studies and pathways to upscaling, *Discover Appl. Sci.*, 2025, **7**, 271.

40 Y. Wang, Y. Chen, J. Harding, H. He, A. Bogaerts and X. Tu, Catalyst-free single-step plasma reforming of CH_4 and CO_2 to higher value oxygenates under ambient conditions, *Chem. Eng. J.*, 2022, **450**, 137860.

41 L. Wang, Y. Wang, L. Fan, H. Xu, B. Liu, J. Zhang, Y. Zhu and X. Tu, Direct conversion of CH_4 and CO_2 to alcohols using plasma catalysis over $Cu/Al(OH)_3$ catalysts, *Chem. Eng. J.*, 2023, **466**, 143347.

42 S. Wang, V. Rohani, T. Ye, P. Dupont, S. Pagnon, M. Sennour and L. Fulcheri, Effect of K-promoter use in iron-based plasma-catalytic conversion of CO_2 and CH_4 into higher value products, *Appl. Catal., A*, 2023, **663**, 119315.

43 J. Li, L. Dou, Y. Gao, X. Hei, F. Yu and T. Shao, Revealing the active sites of the structured Ni-based catalysts for one-step CO_2/CH_4 conversion into oxygenates by plasma-catalysis, *J. CO2 Util.*, 2021, **52**, 101675.

44 L. Fan, Y. Wang, X. Zhai, Q. Yin, J. Zhang, Y. Zhu and L. Wang, Production of oxygenates from CH_4/CO_2 plasma reaction assisted by Ni/HZSM-5 catalyst, *Plasma Chem. Plasma Process.*, 2023, **43**, 1979–1998.

45 M. Z. Salmasi, R. Es'haghian, A. Omidkar and H. Song, Non-thermal plasma-catalytic conversion of biogas to value-added liquid chemicals via $Ni-Fe/Al_2O_3$ catalyst, *Appl. Sci.*, 2025, **15**, 4248.

46 J. Wu, S. Song, L. Wang, R. Li, J. Wen, Y. Guo, J. Ding, D. Mei, H. Wan and G. Guan, Single-Atom Cu anchored polymeric carbon nitride for enhanced one-step plasma-catalytic conversion of CH_4 and CO_2 into acetic acid, *Chem. Eng. J.*, 2024, **499**, 156439.

47 J. Li, L. Dou, Y. Liu, Y. Gao, X. Hu, F. Yu, J. Li, S. Zhang and T. Shao, One-step plasma reforming of CO_2-CH_4 into hydrogen and liquid fuels: the roles of Cu and Fe sites on products distribution, *Fuel Process. Technol.*, 2023, **242**, 107648.

48 C. Qi, Y. Bi, Y. Wang, H. Yu, Y. Tian, P. Zong, Q. Zhang, H. Zhang, M. Wang and T. Xing, Unveiling the mechanism of plasma-catalyzed oxidation of methane to C_{2+} oxygenates over $Cu/UiO-66-NH_2$, *ACS Catal.*, 2024, **14**, 7707–7716.

49 C. Qi, Y. Bi, H. Yu, H. Zhang, Q. Zhang, X. Wang, M. Fan, T. Xing, M. Wang and M. Wu, One-step synthesis of methanol from CH_4 and CO_2 by a plasma synergistic catalyst, *Ind. Eng. Chem. Res.*, 2024, **63**, 9576–9583.

50 L. Wang, L. Fan, Y. Wang, Q. Chen, Y. Zhu and Y. Yi, Tuning selectivity of acetic acid and alcohols by Brønsted and Lewis acid sites in plasma-catalytic CH_4/CO_2 conversion over zeolites, *Appl. Catal., B*, 2024, **350**, 123938.

51 E. C. Neyts, Plasma-surface interactions in plasma catalysis, *Plasma Chem. Plasma Process.*, 2016, **36**, 185–212.

52 P. Mehta, P. Barboun, D. B. Go, J. C. Hicks and W. F. Schneider, Catalysis enabled by plasma activation of strong chemical bonds: A review, *ACS Energy Lett.*, 2019, **4**, 1115–1133.

53 W. Somers, A. Bogaerts, A. Van Duin and E. Neyts, Plasma species interacting with nickel surfaces: Toward an atomic scale understanding of plasma-catalysis, *J. Phys. Chem. C*, 2012, **116**, 20958–20965.

54 H. Koshlak, L. Lobanov, B. Basok, T. Hrabova and P. Goncharov, Plasma photocatalysis: A novel approach for enhanced air disinfection in centralised ventilation systems, *Materials*, 2025, **18**, 1870.

55 H.-H. Kim, Y. Teramoto and A. Ogata, *Plasma-catalyst interactions*, Springer, 2019.

56 K. P. Cheung and C. Chang, Plasma-charging damage: A physical model, *J. Appl. Phys.*, 1994, **75**, 4415–4426.

57 V. Longo, L. De Pasquale, S. Perathoner, G. Centi and C. Genovese, Synergistic effects of light and plasma catalysis on Au-modified TiO_2 nanotube arrays for enhanced non-oxidative coupling of methane, *Catal. Sci. Technol.*, 2025, **15**, 3725–3735.

58 L.-Y. Hsu, W. Ding and G. C. Schatz, Plasmon-coupled resonance energy transfer, *J. Phys. Chem. Lett.*, 2017, **8**, 2357–2367.

59 A. Kumar, P. Choudhary, A. Kumar, P. H. Camargo and V. Krishnan, Recent advances in plasmonic photocatalysis based on TiO_2 and noble metal nanoparticles for energy conversion, environmental remediation, and organic synthesis, *Small*, 2022, **18**, 2101638.

60 E. C. Neyts, K. Ostrikov, M. K. Sunkara and A. Bogaerts, Plasma catalysis: Synergistic effects at the nanoscale, *Chem. Rev.*, 2015, **115**, 13408–13446.

61 Y.-F. Guo, D.-Q. Ye, K.-F. Chen, J.-C. He and W.-L. Chen, Toluene decomposition using a wire-plate dielectric barrier discharge reactor with manganese oxide catalyst in situ, *J. Mol. Catal. A: Chem.*, 2006, **245**, 93–100.

62 H. J. Gallon, X. Tu, M. V. Twigg and J. C. Whitehead, Plasma-assisted methane reduction of a NiO catalyst-Low temperature activation of methane and formation of carbon nanofibres, *Appl. Catal., B*, 2011, **106**, 616–620.

63 X. Tu, H. Gallon and J. Whitehead, Plasma-assisted reduction of a NiO/Al_2O_3 catalyst in atmospheric pressure H_2/Ar dielectric barrier discharge, *Catal. Today*, 2013, **211**, 120–125.

64 S. Shang, G. Liu, X. Chai, X. Tao, X. Li, M. Bai, W. Chu, X. Dai, Y. Zhao and Y. Yin, Research on $Ni/\gamma-Al_2O_3$ catalyst for CO_2 reforming of CH_4 prepared by atmospheric pressure glow discharge plasma jet, *Catal. Today*, 2009, **148**, 268–274.

65 G. V. Bianco, M. M. Giangregorio, P. Capezzuto, M. Losurdo, T.-H. Kim, A. S. Brown and G. Bruno, Plasma-plasmonics synergy in the Ga-catalyzed growth of Si-nanowires, *Mater. Sci. Eng., B*, 2012, **177**, 700–704.

66 J. George and J. Singh, Polaritonic chemistry: Band-selective control of chemical reactions by vibrational strong coupling, *ACS Catal.*, 2023, **13**, 2631–2636.

67 F. van den Bosch, N. Gerrits and J. Meyer, Vibrational excitation in plasma catalysis: How important are dynamical effects?, *EES Catal.*, 2025, **3**, 1257–1271.

68 E. Neyts and A. Bogaerts, Understanding plasma catalysis through modelling and simulation-A review, *J. Phys. D: Appl. Phys.*, 2014, **47**, 224010.

69 J. Khurgin, A. Y. Bykov and A. V. Zayats, Hot-electron dynamics in plasmonic nanostructures: Fundamentals, applications and overlooked aspects, *eLight*, 2024, **4**, 15.

70 G. Yu, J. Qian, P. Zhang, B. Zhang, W. Zhang, W. Yan and G. Liu, Collective excitation of plasmon-coupled Au-nanochain boosts photocatalytic hydrogen evolution of semiconductor, *Nat. Commun.*, 2019, **10**, 4912.

71 J. Van Turnhout, K. Rouwenhorst, L. Lefferts and A. Bogaerts, Plasma catalysis: What is needed to create synergy?, *EES Catal.*, 2025, **3**, 669–693.

72 L. Wang, Q. Yin, X. Zhai and Y. Yi, Recent progresses of plasma-catalytic CH_4/CO_2 conversion to oxygenates: A short review, *Curr. Opin. Green Sustainable Chem.*, 2024, **51**, 100989.

73 Y. Wang, L. Fan, H. Xu, H. Du, H. Xiao, J. Qian, Y. Zhu, X. Tu and L. Wang, Insight into the synthesis of alcohols and acids in plasma-driven conversion of CO_2 and CH_4 over copper-based catalysts, *Appl. Catal., B*, 2022, **315**, 121583.

74 X. Liu, P. Si, Y. Zhang, L. Cui, Y. Feng, T. Wang, M. Zhao, F. Liu and F. Han, Plasma-catalyzed one-step synthesis of alcohols from CO_2 over $Cu/\gamma\text{-}Al_2O_3$ catalyst, *Ind. Eng. Chem. Res.*, 2024, **63**, 1170–1178.

75 P. Ye, G. Miao, D. Ray, Z. Tang and C. Song, Plasma-driven catalytic conversion of biogas to methanol and acetic acid and the role of water in tailoring products, *ACS Sustainable Chem. Eng.*, 2025, **13**, 7532–7540.

76 D. Li, V. Rohani, A. P. Ramaswamy, M. Sennour, F. Georgi, P. Dupont and L. Fulcheri, Orientating the plasma-catalytic conversion of CO_2 and CH_4 toward liquid products by using a composite catalytic bed, *Appl. Catal., A*, 2023, **650**, 119015.

77 D. Mei, M. Sun, S. Liu, P. Zhang, Z. Fang and X. Tu, Plasma-enabled catalytic dry reforming of CH_4 into syngas, hydrocarbons and oxygenates: Insight into the active metals of $\gamma\text{-}Al_2O_3$ supported catalysts, *J. CO2 Util.*, 2023, **67**, 102307.

78 D. Mei, X. Zhu, Y.-L. He, J. D. Yan and X. Tu, Plasma-assisted conversion of CO_2 in a dielectric barrier discharge reactor: Understanding the effect of packing materials, *Plasma Sources Sci. Technol.*, 2014, **24**, 015011.

79 Z. Zhou, F. Yu and J. Ma, Nanoconfinement engineering for enchanced adsorption of carbon materials, metal-organic frameworks, mesoporous silica, MXenes and porous organic polymers: A review, *Environ. Chem. Lett.*, 2022, **20**, 563–595.

80 M. Sofi, M. Hamid, A. Jalil, A. Alhebshi, N. Hassan, M. Bahari and M. Mohamud, Recent advancements of SAPO-34 and ZSM-5 zeolite in converting methanol to olefin: A review, *Arabian J. Sci. Eng.*, 2025, **50**, 3671–3697.

81 D. Mei, G. Duan, J. Fu, S. Liu, R. Zhou, R. Zhou, Z. Fang, P. J. Cullen and K. Ostrikov, CO_2 reforming of CH_4 in single

and double dielectric barrier discharge reactors: Comparison of discharge characteristics and product distribution, *J. CO2 Util.*, 2021, **53**, 101703.

82 M. Y. Ong, S. Nomanbhay, F. Kusumo and P. L. Show, Application of microwave plasma technology to convert carbon dioxide (CO_2) into high value products: A review, *J. Cleaner Prod.*, 2022, **336**, 130447.

83 J.-L. Liu, X. Wang, X.-S. Li, B. Likozar and A.-M. Zhu, CO_2 conversion, utilisation and valorisation in gliding arc plasma reactors, *J. Phys. D: Appl. Phys.*, 2020, **53**, 253001.

84 N. Y. Babaeva and G. V. Naidis, On the efficiency of CO_2 conversion in corona and dielectric-barrier discharges, *Plasma Sources Sci. Technol.*, 2021, **30**, 03LT03.

85 I. Michielsen, Y. Uytdenhouwen, J. Pype, B. Michielsen, J. Mertens, F. Reniers, V. Meynen and A. Bogaerts, CO_2 dissociation in a packed bed DBD reactor: First steps towards a better understanding of plasma catalysis, *Chem. Eng. J.*, 2017, **326**, 477–488.

86 A. Bogaerts, A. Berthelot, S. Heijkers, S. Kolev, R. Snoeckx, S. Sun, G. Trenchev, K. Van Laer and W. Wang, CO_2 conversion by plasma technology: insights from modeling the plasma chemistry and plasma reactor design, *Plasma Sources Sci. Technol.*, 2017, **26**, 063001.

87 Y. Uytdenhouwen, J. Hereijgers, T. Breugelmans, P. Cool and A. Bogaerts, How gas flow design can influence the performance of a DBD plasma reactor for dry reforming of methane, *Chem. Eng. J.*, 2021, **405**, 126618.

88 Y. Feng, Y. Cai, Y. Wang, T. Li, S. Luo, W. Liang, S. Zheng, T. Xie, Q.-Y. Yang, X. Yong, R. Zhou, D. Liu and X. Tu, Enhanced ammonia synthesis using surface microdischarge with metal-loaded nickel foam electrodes, *Chem. Eng. J.*, 2025, **510**, 161553.

89 P. Ye, J. Wang, Z. Yuan, G. Miao and C. Song, Enhancing CO_2 splitting via plasma catalysis: Impact of electrode design and catalyst, *Energy Fuels*, 2025, **39**, 22335–22341.

90 P. Bruggeman and C. Leys, Non-thermal plasmas in and in contact with liquids, *J. Phys. D: Appl. Phys.*, 2009, **42**, 053001.

91 H. Wang, R. J. Wandell, K. Tachibana, J. Voráč and B. R. Locke, The influence of liquid conductivity on electrical breakdown and hydrogen peroxide production in a nanosecond pulsed plasma discharge generated in a water-film plasma reactor, *J. Phys. D: Appl. Phys.*, 2018, **52**, 075201.

92 D.-Y. Kim, S. Furukawa, S. Takakusagi, H.-H. Kim and T. Nozaki, Synergistic plasma catalysis for CO_2 conversion: Mechanistic insights, advanced characterization, and rational design strategies, *ACS Catal.*, 2025, **15**, 19424–19444.

93 J. W. Gregory, N. Pourali, Y. Gong, R. I. Walton, V. Hessel and E. V. Rebrov, Development of an Ir/TiO_2 catalytic coating for plasma assisted hydrogenation of CO_2 to CH_4, *Appl. Catal., A*, 2024, **675**, 119639.

94 M. Smolarek, H. Kierzkowska-Pawlak, R. Kapica, M. Fronczak, M. Sitarz, M. Leśniak and J. Tyczkowski, Cold plasma synthesis and testing of NiO_X-based thin-film catalysts for CO_2 methanation, *Catalysts*, 2021, **11**, 905.